nature cardiovascular research

Article

https://doi.org/10.1038/s44161-025-00672-8

Transcriptional changes of the extracellular matrix in chronic thromboembolic pulmonary hypertension govern right ventricle remodeling and recovery

Received: 16 July 2023

Accepted: 13 May 2025

Published online: 4 July 2025

Check for updates

A list of authors and their affiliations appears at the end of the paper

Chronic thromboembolic pulmonary hypertension (CTEPH) leads to progressive right ventricular (RV) dysfunction. Pulmonary endarterectomy (PEA) is an established treatment for these patients; however, the molecular mechanisms underlying RV remodeling and recovery remain poorly understood. Here we show that RNA sequencing and histological analysis of RV free wall and septal biopsies from patients with CTEPH reveal extracellular matrix enrichment and cytoskeletal remodeling before PEA. These changes were consistent across an exploratory and confirmatory cohort. Post-PEA samples showed reversal of both histological and transcriptional abnormalities. Key signaling molecules—ANKRD1, IL7R and SERPINE1—were implicated in fibrotic and proliferative pathways, as confirmed in human tissues and experimental models. Our findings identify a reversible gene expression and structural remodeling signature in the RV, linking hemodynamic unloading with molecular recovery. These insights suggest potential therapeutic targets to modulate maladaptive RV remodeling in CTEPH and improve outcomes beyond surgical intervention.

Right ventricular (RV) remodeling is a hallmark of pulmonary hypertension (PH), substantially affecting RV function and clinical outcomes[1,2]. A better understanding of the complex functional and structural adaptive and maladaptive processes is crucial, as RV remodeling may be reversible[3,4]. However, the molecular mechanisms driving the transition between functional and failing RV states remain poorly understood. Recent studies using omics technologies have begun to elucidate transcriptomic profiles associated with RV adaptation in pulmonary arterial hypertension (PAH, group 1 PH)[5–7].

Chronic thromboembolic pulmonary hypertension (CTEPH), a group 4 PH subtype, arises from unresolved thromboemboli that obstruct pulmonary vessels, promoting vascular remodeling and RV failure if untreated[8–10]. The gold standard treatment for CTEPH is pulmonary endarterectomy (PEA), which is so far the only potential cure for these patients and usually leads to a far-reaching normalization of pulmonary hemodynamics, with recovery of the RV after PEA being observed in the majority of patients[4,11]. Yet, the degree of post-PEA recovery varies[12–14], and the underlying molecular and structural mechanisms are not fully characterized.

By contrast, reverse remodeling of the left ventricle (LV) in the context of heart failure has been extensively studied. It comprises restoration of LV chamber geometry with a leftward shift of the end-diastolic pressure–volume relationship, linked with normalization of myocardial cell size and changes of various molecular, metabolic and extracellular matrix (ECM)-related properties toward physical homeostasis[15–17].

CTEPH offers a rare opportunity to study RV remodeling in humans at the intraindividual level, with access to myocardial biopsies before and after surgical intervention[14,18,19]. In our study, RV free wall and septal biopsies from patients with CTEPH undergoing PEA (prePEA) were analyzed to investigate transcriptomic and structural remodeling compared with controls. Patients were stratified by clinical severity based on European Society of Cardiology (ESC) and European Respiratory

e-mail: c.liebetrau@ccb.de; Soni.Pullamsetti@innere.med.uni-giessen.de

https://doi.org/10.1038/s44161-025-00672-8

a

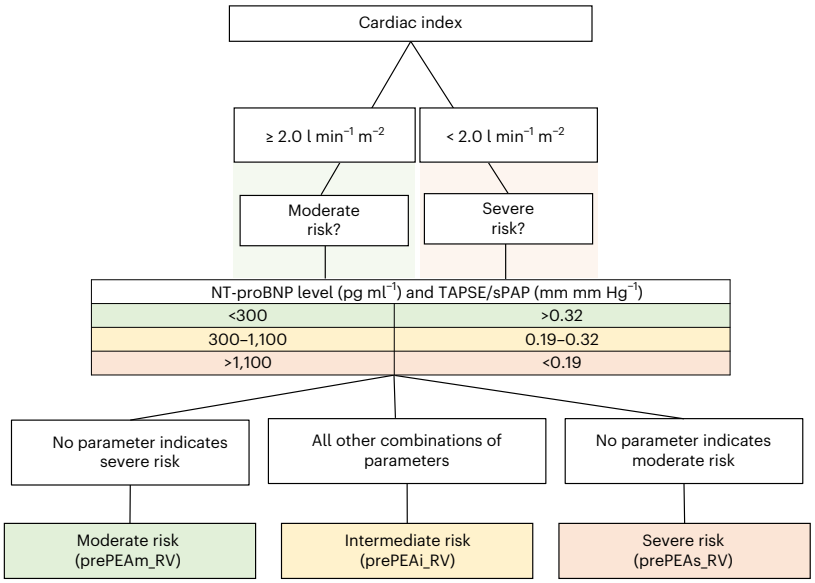

b

		Parameter	Total (*n* = 14)	A-prePEAm_RV (*n* = 4)	A-prePEAi_RV (*n* = 5)	A-prePEAs_RV (*n* = 5)	*P* value[a]	*P* value[b]	*P* value[c]
Exploratory cohort	RNA-seq	NT-proBNP (pg ml^{-1})	810.7 (145.3–1,859)	113.4 (43.75–390.9)	1112 (555.3–1,943)	1,466 (544–3,825)		0.03	
		CI (l min^{-1} m^{-2})	2.25 ± 0.47	2.4 ± 0.35	2.25 ± 0.44	1.79 ± 0.16		0.01	0.006
		TAPSE/sPAP (mm mm Hg^{-1})	0.23 (0.14–0.35)	0.43 (0.35–0.55)	0.21 (0.14-0.24)	0.16 (0.12–0.24)	0.01	0.01	
		Parameter	Total (*n* = 71)	B-prePEAm_RV (*n* = 30)	B-prePEAi_RV (*n* = 23)	B-prePEAs_RV (*n* = 18)	*P* value[a]	*P* value[b]	*P* value[c]
Confirmatory cohort	RNA-seq	NT-proBNP (pg ml^{-1})	1,046 (354.7–2,047)	361.8 (133.5–702.7)	1,890 (1,312–2,620)	2,079 (1254–4756)	<0.0001	<0.0001	
		CI (l min^{-1} m^{-2})	2.29 ± 0.57	2.66 ± 0.44	2.30 ± 0.45	1.63 ± 0.20	0.007	<0.0001	<0.0001
		TAPSE/sPAP (mm mm Hg^{-1})	0.25 (0.19–0.35)	0.34 (0.23–0.47)	0.21 (0.18–0.33)	0.22 (0.16–0.25)	0.002	0.0001	
	Histological assessment	Parameter	Total (*n* = 43)	B-prePEAm_RV (*n* = 18)	B-prePEAi_RV (*n* = 18)	B-prePEAs_RV (*n* = 8)	*P* value[a]	*P* value[b]	*P* value[c]
		NT-proBNP (pg ml^{-1})	748.5 (334.3–2,203)	357.6 (153.7–613.6)	1,821 (771.2–3,310)	2,125 (634.9–5,836)	<0.0001	0.001	
		CI (l min^{-1} m^{-2})	2.24 ± 0.45	2.49 ± 0.33	2.20 ± 0.46	1.75 ± 0.18	0.04	<0.0001	0.01
		TAPSE/sPAP (mm mm Hg^{-1})	0.26 (0.18–0.35)	0.31 (0.22–0.46)	0.24 (0.18–0.32)	0.18 (0.13–0.27)	0.03	0.03	

c

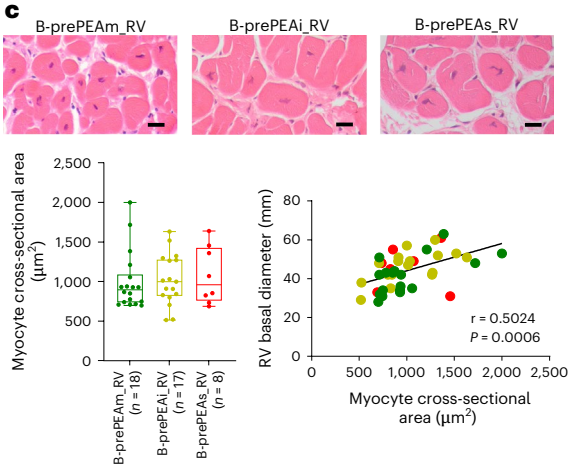

d

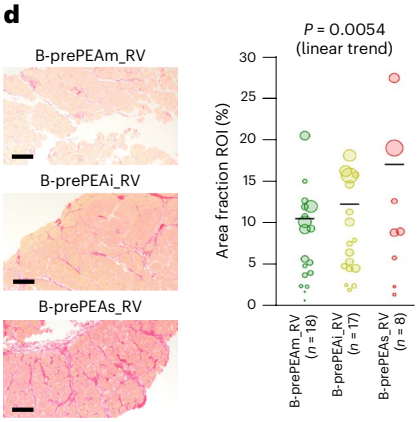

Fig. 1 | Classification of patients with CTEPH. a, The flowchart shows the algorithm for risk stratification in patients with CTEPH. **b**, Classification of patients with CTEPH before PEA based on their clinical parameters and ESC/ERS guidelines in the exploratory cohort (A-prePEA_RV, $n = 14$) and confirmatory cohort for RNA-seq profiling (B-prePEA_RV, $n = 71$) and for histological assessment (B-prePEA_RV, $n = 43$). Data are presented as median (IQR) (NT-proBNP and TAPSE/sPAP) or mean ± s.d. (CI), and the *P* value was calculated using the two-tailed Mann–Whitney test or unpaired two-tailed *t*-test, respectively. The *P* values correspond to the following comparisons: [a]A-prePEAm_RV versus A-prePEAi_RV/B-prePEAm_RV versus B-prePEAi_RV, [b]for A-prePEAm_RV versus A-prePEAs_RV/B-prePEAm_RV versus B-prePEAs_RV and [c]for A-prePEAi_RV versus A-prePEAs_RV/B-prePEAi_RV versus B-prePEAs_RV. **c**, Representative images and quantification of the cross-sectional areas of RV myocytes within H&E-stained tissue sections were analyzed in the confirmatory cohort of patients with CTEPH at prePEA (B-prePEA_RV, $n = 43$). Data are presented as mean ± SEM, and *P* values were calculated by one-way ANOVA followed by Tukey's multiple-comparison test. Pearson correlation was conducted between the RV basal diameter and myocyte cross-sectional area. The boxes show the IQR (25th to 75th percentile), and the central bands indicate the median. The whiskers extend to 1.5 times the IQR above and below the box. Scale bars, 20 μm. **d**, Representative images and corresponding quantification of Sirius red-stained RV sections depicting the percentage of area fraction (ROI) in different risk groups of patients with CTEPH from the confirmatory cohort. The categorization includes moderate-risk (B-prePEAm_RV, $n = 18$ patients with $n = 79$ fibrosis tissue sections), intermediate-risk (B-prePEAi_RV, $n = 17$ patients with $n = 68$ fibrosis tissue sections) and severe-risk (B-prePEAs_RV, $n = 8$ patients with $n = 28$ fibrosis tissue sections) groups. The differences in the area fractions between the different risk groups were defined with a quasi-binomial model using the weights, and the *P* value was calculated using chi-squared test. Scale bars, 100 μm.

Society (ERS) criteria, and follow-up post-PEA surgery (postPEA) allowed for intraindividual comparisons of recovery. Furthermore, RV transcriptomic profiles were compared with datasets from human left heart failure and mouse models of pulmonary artery banding (PAB) and de-banding to identify common and distinct molecular features.

Results

ESC/ERS-based CTEPH groups show RV structural and gene changes

In this study, patients with CTEPH before PEA (prePEA) were categorized into different risk groups in the exploratory (A-prePEA_RV, $n = 14$) and confirmatory (B-prePEA_RV, $n = 88$) cohorts based on their clinical parameters and the ESC/ERS guidelines[8]. Risk stratification was guided by a flowchart-based algorithm incorporating three key parameters—cardiac index (CI), N-terminal pro-brain natriuretic peptide (NT-proBNP) level, and the tricuspid annular plane systolic excursion to systolic pulmonary arterial pressure (TAPSE/sPAP) ratio—along with specific value ranges. Patients were first divided based on a CI threshold of 2.0 l min^{-1} m^{-2}. In the moderate-risk group (prePEAm) (CI ≥ 2.0), neither NT-proBNP nor TAPSE/sPAP values fell within the severe-risk range (NT-proBNP > 1100 pg ml^{-1} or TAPSE/sPAP <0.19 mm mm Hg^{-1}). In the severe-risk group (prePEAs) (CI < 2.0), no parameter indicated moderate-risk values (NT-proBNP <300 pg ml^{-1} or TAPSE/sPAP > 0.32 mm mm Hg^{-1}). The intermediate-risk group (prePEAi) included all other combinations that did not meet the exclusive criteria for either moderate or severe risk (Fig. 1a,b, Table 1, Supplementary Tables 1 and 2, and Methods).

In the confirmatory cohort, RV histology revealed a significant correlation between myocyte cross-sectional area and RV basal diameter (Fig. 1c and Supplementary Table 2). Notably, the severe-risk group showed increased RV fibrosis compared with the intermediate- and moderate-risk groups (Fig. 1d and Supplementary Table 2). To determine whether the ESC/ERS-based subgrouping of patients with CTEPH also correlates with transcriptomic changes in the right ventricle, RNA-sequencing (RNA-seq) was performed on the RV biopsies of the exploratory cohort, that is, A-prePEA_RV before PEA (Extended Data Fig. 1a and Supplementary Table 1). Principal component analysis (PCA) revealed clear separation among the risk groups, indicating transcriptomic divergence (Extended Data Fig. 1b and Supplementary Fig. 1). Differential gene expression analysis identified 814 dysregulated genes in the severe-risk group and 279 in the intermediate-risk group compared with the moderate-risk group (Extended Data Fig. 1c–e). Of these, 34 and 567 genes were uniquely expressed in the intermediate-risk and severe-risk groups, respectively (Extended Data Fig. 1f).

The top 50 differentially expressed genes (DEGs) in the severe-risk and intermediate-risk groups compared with the moderate-risk group include the heart-disease-associated genes, that is, proenkephalin (*PENK*), transforming growth factor beta 2 (*TGFB2*) and natriuretic peptide precursor A (*NPPA*) and B (*NPPB*). ECM-related genes include tenascin-C (*TNC*), periostin (*POSTN*) as a secreted ECM protein and collagen type IX alpha 1 chain *(COL9A1)* (Supplementary Fig. 2a,b). Gene Ontology (GO) enrichment analysis highlighted ECM-related terms among the top 20 overrepresented clusters of terms in the intermediate-risk and severe-risk groups, including 'cell adhesion molecule binding', 'AGE-RAGE signaling pathway', 'cytoskeleton in muscle cells', 'NABA MATRISOME ASSOCIATED', 'enzyme-linked receptor protein signaling pathway' and 'extracellular matrix' (Extended Data Fig. 1g and Supplementary Fig. 3). Additional pathways such as 'response to estradiol', 'response to hypoxia' and 'regulation of cytoskeletal organization' were enriched exclusively in the severe-risk group (Supplementary Fig. 3).

RV gene changes by risk group in the CTEPH confirmatory cohort

To validate the association between clinical parameters and transcriptional changes observed in the exploratory cohort, we performed RNA-seq on the RV of 71 patients out of 88 in the confirmatory cohort. Patients were again stratified into moderate-risk (B-prePEAm_RV, $n = 30$), intermediate-risk (B-prePEAi_RV, $n = 23$) and severe-risk (B-prePEAs_RV, $n = 18$) groups based on the same scoring system (Figs. 1a,b and 2a, and Table 1). Compared with the moderate-risk group, the intermediate- and severe-risk groups showed increased NT-proBNP, sPAP, mean pulmonary artery pressure (mPAP), pulmonary vascular resistance (PVR) and RV basal diameter, and reduced maximum oxygen consumption (VO_2max), CI, cardiac output (CO) and TAPSE/sPAP (Table 1).

PCA separated moderate- and severe-risk groups, while the intermediate-risk group showed greater heterogeneity (Fig. 2b). DEG analysis revealed 358 and 88 dysregulated genes in the severe- and intermediate-risk groups, respectively, compared with the moderate-risk group. Only 15 DEGs were found between the intermediate- and severe-risk groups, suggesting limited transcriptomic divergence despite clinical differences (Fig. 2c–e and Table 1).

Venn diagrams and GO term enrichment analysis for both cohorts showed shared and unique genes and pathways. GO terms enriched in the severe-risk group included 'enzyme-linked receptor protein signaling pathway', 'cytoskeleton', 'positive regulation of cell motility', 'NABA MATRISOME ASSOCIATED' and 'adipogenesis'—consistent with findings from the exploratory cohort (Fig. 2f,g and Extended Data Fig. 2). Several highly regulated genes within these GO terms—including *COMP* (cartilage oligomeric matrix protein), *COLQ* (acetylcholinesterase collagenic tail peptide), *CD38* (cluster of differentiation 38), *SEZ6L* (seizure related 6 homolog like), *CDH11* (cadherin 11), *CCN2* (cellular communication network factor 2), *CCDC80* (coiled-coil domain-containing protein 80), *CRACD* (capping protein inhibiting regulator of actin dynamics), *SERPINE1* (serpin family E member 1), *LTBP2* (latent transforming growth factor beta binding protein 2), *NPPB* and *NPPA*—show an association with disease severity.

CTEPH versus control and LHF reveals RV failure-related genes

To explore molecular mechanisms of RV remodeling in CTEPH, transcriptomic profiles of the B-prePEA_collective RV cohort ($n = 71$; moderate $n = 30$, intermediate $n = 23$ and severe $n = 18$) were compared with those of a normal control group (Control_RV, $n = 10$) (Fig. 3a). PCA plots showed clear separation between all prePEA subgroups and Control_RV (Fig. 3b). Global gene expression correlations are shown in Supplementary Fig. 4a–c. RNA-seq revealed over 4,000 DEGs in all prePEA subgroups compared with controls (Fig. 3c–e). Venn diagrams showed both shared and unique DEGs in each group (Fig. 3f and Supplementary Fig. 5a–c), with 547, 288 and 502 genes uniquely regulated in the moderate-, intermediate- and severe-risk groups, respectively.

GO analysis identified enriched terms such as 'NABA MATRISOME ASSOCIATED', 'extracellular matrix', 'regulation of cell activation', 'positive regulation of immune response', 'cellular response to cytokine stimulus' and 'neutrophil degranulation' in prePEA subgroups compared with Control_RV (Fig. 3g and Extended Data Fig. 3). Notably, inflammatory-related GO terms showed increased log fold changes (FCs) with disease severity.

To assess RV failure-specific transcriptional signatures, data from two public heart failure studies were incorporated. From GSE11625020 (ref. 20), we reanalyzed normalized counts from LV tissue of patients with dilated ($n = 37$) or ischemic cardiomyopathy ($n = 13$) versus non-failing controls ($n = 14$) using R package limma[21] with the default setting. These were compared with RV samples from the confirmatory cohort (B-prePEAs_RV versus B-prePEAm_RV), processed identically. Gene expression profiles showed a modest but significant correlation ($r = 0.39$ $\log_2$(FC), $P < 0.0001$), with 57 DEGs overlapping (≥2-fold, false discovery rate (FDR) ≤ 5%) and 4 (7%) regulated in opposite directions (Supplementary Fig. 6a).

Table 1 | Clinical characteristics of the patients with CTEPH in the prePEA confirmatory cohort

Parameter	Total (*n*=71)	B-prePEAm_RV (*n*=30)	B-prePEAi_RV (*n*=23)	B-prePEAs_RV (*n*=18)	*P* value[b]	*P* value[c]	*P* value[d]
General characteristics							
Female gender, *n* (%)	22 (30.99)	11 (36.67)	7 (30.43)	4 (22.22)			
Age at PEA (years)	58.7±14.7	57.7±15	59.6±14	59.5±15.8			
BMI (kg m^{-2})	27.81±6.01	28.18±5.25	27.41±7.01	27.71±6.16			
Laboratory							
GFR (ml min^{-1} 1.73 m^{-2})[a]	80.29 (63.71–92.57)	89.26 (79.40–96.68)	78.33 (62.53–96.86)	71.1 (49.19–82.17)		0.007	
Creatinine (µmol l^{-1})[a]	0.96 (0.82–1.12)	0.9 (0.72–1)	1.03 (0.82–1.2)	1.14 (0.99–1.2)		0.002	
NT-proBNP (pg ml^{-1})[a]	1,046 (354.7–2,047)	361.8 (133.5–702.7)	1,890 (1,312–2,620)	2,079 (1,254–4,756)	<0.0001	<0.0001	
Functional status							
6-MWD (m)	415.8±110.13	452.6±90.85	401.7±111.2	336±128.7			
WHO FC, *n* (%)							
I	0 (0)	0 (0)	0 (0)	0 (0)			
II	8 (11.3)	5 (16.6)	4 (17.4)	0 (0)			
III	50 (70.4)	20 (66.6)	16 (69.6)	13 (72.2)			
IV	13 (18.3)	5 (16.7)	3 (13)	5 (27.8)			
VO_2max (ml min^{-1} kg^{-1})	11.89±4.01	15.21±4.79	10.6±2.8	10.13±2.43	0.008	0.008	
Hemodynamics							
sPAP (mm Hg)	72.39±19.33	63.27±19.02	81.48±18.13	76±14.95		0.04	0.001
mPAP (mm Hg)	41.42±10.21	36.07±9.34	45.74±9.88	44.83±8.12	0.001	0.006	
mRAP (mm Hg)	7.4±3.81	6.33±2.63	6.84±4.1	10.71±4.03		0.02	
PVR (WU)	7.54±3.16	5.72±2.59	7.7±1.98	10.33±3.14	0.03	<0.0001	0.008
CI (l min^{-1} m^{-2})	2.29±0.57	2.66±0.44	2.30±0.45	1.63±0.20	0.007	<0.0001	<0.0001
CO (l min^{-1})	4.54±1.24	5.30±1.13	4.45±0.93	3.47±0.78	0.02	<0.0001	0.002
Echocardiography							
RV basal diameter (mm)	44.25±8.1	38.83±9.96	47.45±8.4	49.35±11.42	0.002	0.0006	
LVEF (%)[a]	60 (55–60)	60 (55–60)	57 (55–60)	55 (55–60)			
TAPSE (mm)[a]	19 (16–23)	20.5 (19–24.5)	18 (15–22)	15.5 (11.75–18.25)		<0.0001	
TAPSE/sPAP (mm mm Hg^{-1})[a]	0.25 (0.19–0.35)	0.34 (0.23–0.47)	0.21 (0.18–0.33)	0.22 (0.16–0.25)	0.002	0.0001	

Data are presented as *n* (%), median (IQR) or mean±s.d. BMI, body mass index; GFR, glomerular filtration rate; 6-MWD, 6-min-walk-test distance; WHO FC, World Health Organization Functional Class; WU, wood units; LVEF, left ventricular ejection fraction. [a]Median (IQR). [b]B-prePEAm_RV versus B-prePEAi_RV. [c]B-prePEAm_RV versus B-prePEAs_RV. [d]B-prePEAi_RV versus B-prePEAs_RV.

In addition, comparison with a meta-analysis of 16 left heart failure (LHF) studies[22] revealed that 143 genes (~40%) overlapped with right ventricular failure/right ventricular hypertrophy (RVF/RVH) DEGs, indicating that right heart failure (RHF) transcriptional responses are largely distinct from those in LHF (Supplementary Fig. 6b).

Septum shows molecular alterations pre- and post-PEA

To determine the effect of PEA on the gene expression profile of the septum, septal biopsies were taken using catheters placed in the RV cavity of three pre-PEA patients of the confirmatory cohort. The expression profiles of these samples (B-prePEA_septum) were compared with those of control septa (Control_septum, $n = 10$) (Fig. 4a). PCA revealed clear separation between B-prePEA_septum and Control_septum. RNA-seq identified 3,323 DEGs in the B-prePEA_septum versus controls (Fig. 4b–d), indicating interventricular septal remodeling due to RV pressure overload in CTEPH.

Next, we compared (1) septum and RV free wall gene expression at baseline, (2) septum changes pre- versus post-PEA and (3) overall RV and septal remodeling. We analyzed RNA-seq data from matched septal and RV biopsies (Supplementary Table 3). There were 404 DEGs between B-prePEA_septum and B-prePEA_RV, and 205 DEGs between B-prePEA_RV and B-postPEA_septum (Fig. 4e,f). The top 50 DEGs for each comparison are shown in Fig. 4g,h. A Venn diagram revealed 1,400 co-regulated genes out of 3,288 in the RV and septum at baseline compared with the control (Fig. 4i).

Post-PEA, 21 DEGs were found in the septum versus pre-PEA, with changes in ECM and cytoskeletal terms, but not in muscle contraction or cell adhesion pathways (Extended Data Fig. 4a–d). Pathway analysis indicated strong enrichment of ECM-related and cardiac muscle development pathways in both the septum and right ventricle before PEA, including actin filament processes, cytoskeleton organization and muscle contraction (Extended Data Figs. 4d and 5).

Intraindividual RNA-seq reveals ECM and immune changes post-PEA

As due to clinical restrictions a direct comparison between prePEA and postPEA septal biopsies could be performed only in three patients with CTEPH, we extended this study to another 21 patients with CTEPH in whom the RV free wall biopsy was taken before PEA (B-prePEA_RV) and the septum biopsy was taken 12 months after PEA (B-postPEA_septum). PEA significantly reduced mPAP, PVR, sPAP, RV basal diameter and NT-proBNP, while the TAPSE/sPAP ratio and CO increased (Fig. 5a and Supplementary Table 4).

https://doi.org/10.1038/s44161-025-00672-8

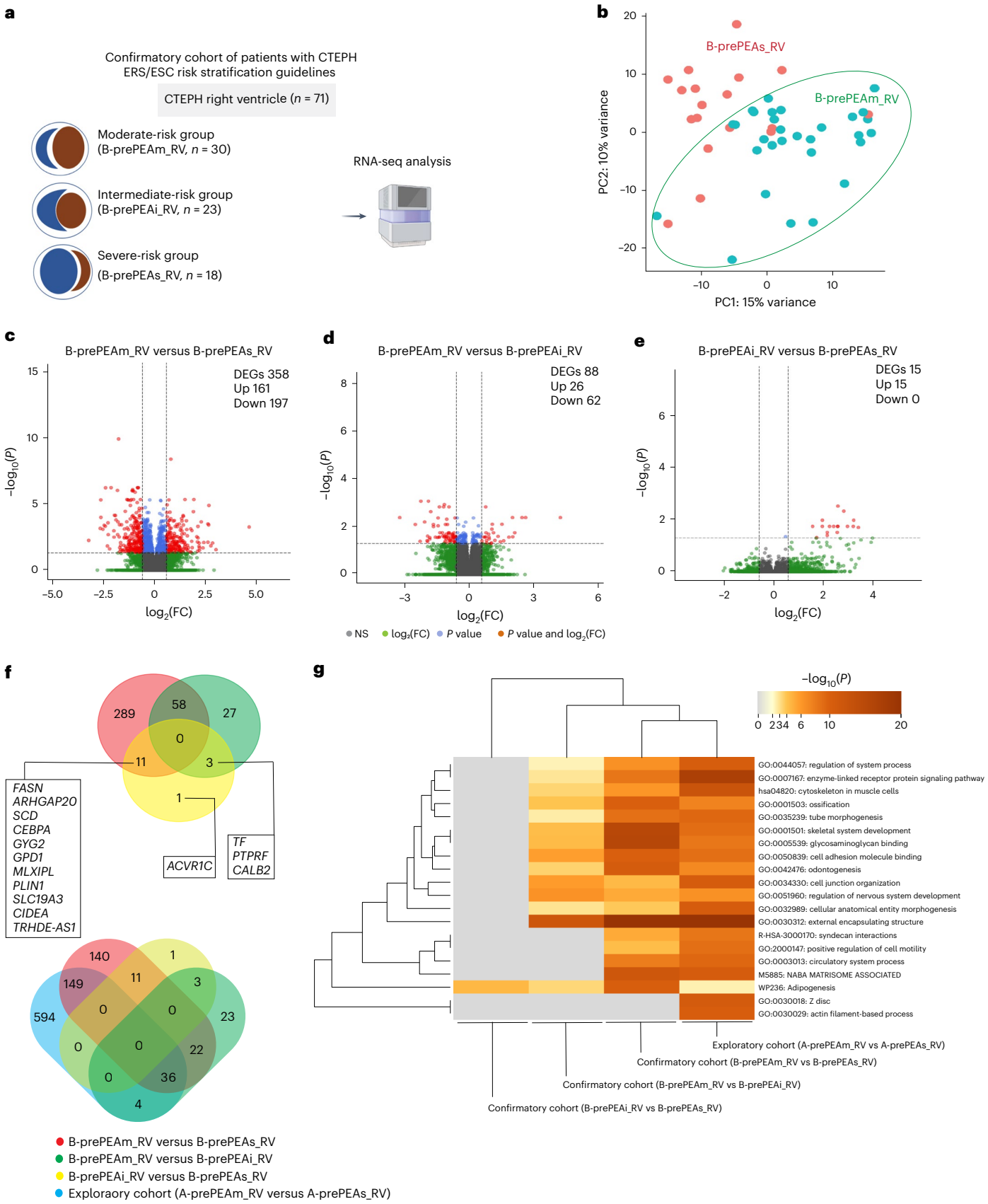

A global gene expression correlation matrix is shown in Supplementary Fig. 7. Patients were stratified into moderate-, intermediate- and severe-risk groups per ESC/ERS guidelines (Fig. 5a). A PCA showed clear separation between the right ventricle and septum by PC1 (Fig. 5b). RNA-seq revealed 1,492 DEGs between B-postPEA_septum and B-prePEA_RV (Fig. 5c). A comparison of postPEA septum samples with prePEA RV samples identified 1,082, 701 and 1,026 DEGs in the moderate-, intermediate- and severe-risk groups, respectively

Fig. 2 | Transcriptomic profiling of the right ventricle in the confirmatory cohorts of patients with CTEPH. a, RNA-seq analysis was performed on the RV tissue of patients with CTEPH ($n = 71$) in the confirmatory cohort. Patients were stratified into moderate-risk (B-prePEAm_RV, $n = 30$), intermediate-risk (B-prePEAi_RV, $n = 23$) and severe-risk (B-prePEAs_RV, $n = 18$) groups based on their clinical parameters and the ESC/ERS guidelines. **b**, PCA plot illustrating the RV transcriptomic profiles of patients in the B-prePEAm_RV and B-prePEAs_RV groups. Each patient in the B-prePEAs_RV group is represented by a red circle, and each patient in the B-prePEAm_RV group is represented by a green circle. **c**–**e**, Volcano plots showing the distribution of the genes in B-prePEAm_RV versus B-prePEAs_RV (**c**), B-prePEAm_RV versus B-prePEAi_RV (**d**) and B-prePEAi_RV versus B-prePEAs_RV (**e**). The significant DEGs (base mean ≥ 5; $|\log_2(FC)| \geq 0.585$; *P*-adjusted value (P_{adj}) ≤ 0.05, two sided) were discriminated based on $P < 0.05$ and $|\log_2(FC)| > 0.585$ (red dots), with genes solely significant in *P* value represented by blue dots, those solely significant in $\log_2(FC)$ represented by green dots and non-significant (NS) genes represented by gray dots. **f**, Venn diagrams of DEGs illustrate the common and distinct DEGs among the three groups of B-prePEAm_RV versus B-prePEAs_RV, B-prePEAm_RV versus B-prePEAi_RV and B-prePEAi_RV versus B-prePEAs_RV in the confirmatory cohort of patients with CTEPH. The counts of overlapping and distinct DEGs across four groups (A-prePEAm_RV versus A-prePEAs_RV, B-prePEAm_RV versus B-prePEAs_RV, B-prePEAi_RV versus B-prePEAs_RV and B-prePEAm_RV versus B-prePEAi_RV) are shown. **g**, Heatmap showing the top 20 overrepresented clusters of terms for all the DEGs between the following comparisons: B-prePEAi_RV versus B-prePEAs_RV, B-prePEAm_RV versus B-prePEAi_RV, B-prePEAm_RV versus B-prePEAs_RV and A-prePEAm_RV versus A-prePEAs_RV. Panel **a** created with BioRender.com.

(Fig. 5d–f). Venn diagrams show 292 commonly regulated DEGs across all subgroups (Fig. 5g), with the top 50 DEGs shown in Supplementary Fig. 8a–d.

Pathway enrichment in B-postPEA_septum versus B-prePEA_RV revealed upregulation of tube morphogenesis, ECM remodeling, cell motility, actin filament processes, PI3K-Akt signaling and positive regulation of cell death. By contrast, immune-related pathways such as phagosome and inflammatory response were absent in B-postPEAi_septum versus B-prePEAi_RV (Fig. 5h and Extended Data Fig. 6), suggesting gene expression changes consistent with reverse remodeling after PEA.

To explore whether reverse remodeling is linked to pressure unloading, we compared these data with mouse models of PAB and de-banding. Mice underwent sham surgery (Sham, $n = 3$), PAB with chronic RV pressure overload ($n = 3$) or gradual pressure unloading (De-PAB or Rapide, $n = 3$)[23]. Shared and specific DEGs and pathways between PAB versus Sham and PAB versus Rapide are shown in Extended Data Fig. 7a,b and Supplementary Fig. 9 ($|\log_2(FC)| \geq 2$, $P \leq 0.01$). Muscle structure development was enriched in both comparisons. However, 2,707 DEGs in PAB versus Rapide revealed GO terms related to organelle organization, mRNA metabolism and mitochondrial and nuclear catabolism, indicating broad metabolic changes during unloading. Comparing these mouse data with human CTEPH datasets revealed that ~8–10% of DEGs were shared post-PEA and post-de-banding (Extended Data Fig. 7c–g).

Intraindividual histology shows reverse remodeling post-PEA

As RNA-seq data revealed transcriptomic differences in the septum of patients with CTEPH that change after PEA, we assessed whether these are reflected in histological remodeling. Hypertrophy, fibrosis and vascularization were analyzed in B-prePEA_RV samples ($n = 13$) and septal biopsies 12 months post-PEA ($n = 13$) (Supplementary Table 5). Fibrosis was significantly reduced post-PEA (Extended Data Fig. 8a), and the myocyte cross-sectional area was decreased in paired post-PEA septum samples (Extended Data Fig. 8b). This area significantly correlated with RV basal diameter, NT-proBNP, TAPSE/sPAP, sPAP, PVR and mPAP (Extended Data Fig. 8c). In addition, capillary density relative to myocardial volume was significantly higher in post-PEA septum samples compared with pre-PEA RV biopsies (Extended Data Fig. 8d and Supplementary Table 6), supporting reverse structural remodeling after PEA.

SERPINE1, *IL7R* and *ANKRD1* link to RV recovery and PEA response

Three genes—serpin family E member 1 (*SERPINE1*), interleukin 7 receptor (*IL7R*) and ankyrin repeat domain 1 (*ANKRD1*)—were selected to investigate whether their expression is altered post-PEA and how this regulation correlates with clinical parameters. *SERPINE1* is one of the genes that play an important role in the top-regulated ECM-related terms and pathways. *SERPINE1* is associated with the external encapsulation structure, extracellular matrix, collagen-containing extracellular matrix, matrisome and tube morphogenesis. *SERPINE1* expression was higher in the severe-risk group than in the moderate-risk group and correlated significantly with the clinical parameters of patients with CTEPH before PEA (Fig. 6a,b). *ANKRD1* is mainly associated with the major terms and pathways related to cardiac muscle, including actin filament-based processes and actin cytoskeleton organization, as well as muscle and heart development, particularly in comparisons between B-prePEA_septum and both Control_septum and B-prePEA_RV. The expression of *ANKRD1* was significantly correlated with the CI and NT-proBNP (Fig. 6a,c). The *IL7R* gene plays a crucial role in key signaling pathways, including the PI3K-Akt and PI3K-Akt-mTOR pathways, which are essential for focal adhesion and cell morphogenesis. Gene expression of *ANKRD1*, *SERPINE1* and *IL7R* was found to be significantly lower expressed in B-postPEA_septum samples than in B-prePEA_RV samples (Fig. 6a), with the expression changes being correlated with the hemodynamic changes induced by PEA in these patients (Supplementary Fig. 10a–c).

SERPINE1, *IL7R* and *ANKRD1* respond to RV pressure overload

To identify the cell types expressing *SERPINE1*, *IL7R* and *ANKRD1*, the Human Cardiac Cell Atlas (v2) was analyzed[24]. Uniform manifold approximation and projection showed the distribution of these genes across 704,296 individual cells spanning 12 cardiac cell types (Supplementary Fig. 11a). In addition, human heart atlas data using Visium technology mapped the expression of these genes in three normal RV tissues (>55 years, 5,039 cells) and four normal septal tissues (>45 years,

Fig. 3 | Comparing the transcriptomic profiling of the right ventricle in patients with CTEPH of the confirmatory cohort with that of the control right ventricle. a, In the confirmatory cohort of patients with CTEPH, RNA-seq was performed on RV tissue (B-prePEA_RV, $n = 71$). The patients at prePEA were classified based on their clinical parameters and ESC/ERS guidelines into B-prePEAm_RV ($n = 30$), B-prePEAi_RV ($n = 23$) and B-prePEAs_RV ($n = 18$). In addition, RNA-seq analysis was performed on Control_RV ($n = 10$). **b**, PCA plots depicting the RV transcriptomic profiles in the following groups: B-prePEAm_RV ($n = 30$) and Control_RV ($n = 10$), B-prePEAi_RV ($n = 23$) and Control_RV ($n = 10$), and B-prePEAs_RV ($n = 18$) and Control_RV ($n = 10$) for each comparison. In each PCA plot, the encircled blue dots represent the right ventricles of patients with CTEPH, while the Control_RVs are shown with red dots. **c**–**e**, Volcano plot representing the gene distribution for different comparisons: B-prePEAm_RV versus Control_RV (**c**), B-prePEAi_RV versus Control_RV (**d**) and B-prePEAs_RV versus Control_RV (**e**). The significant DEGs were selected based on the following criteria: base mean ≥ 5; $|\log_2(FC)| \geq 0.585$; $P_{adj} \leq 0.05$, two-sided. Classification of the significant DEGs was performed based on $P < 0.05$ and $|\log_2(FC)| > 0.585$ (indicated by red dots), only *P* value (indicated by blue dots), $\log_2(FC)$ (indicated by green dots) and not significant (indicated by gray dots). **f**, Venn diagram showing the overlap and distinct DEGs between three distinct groups: B-prePEAm_RV versus Control_RV, B-prePEAi_RV versus Control_RV and B-prePEAs_RV versus Control_RV. **g**, Heatmap visualizing the top 20 overrepresented clusters of terms among various comparisons: B-prePEAm_RV versus Control_RV, B-prePEAi_RV versus Control_RV and B-prePEAs_RV versus Control_RV.

8,643 cells) (Supplementary Fig. 11b,c)[25]. Correlation matrices of *SERPINE1*, *IL7R* and *ANKRD1* with virtual reference transcripts across myocardial cell types were generated using Human Protein Atlas data (Supplementary Fig. 12a–c). Expression of these genes and cell-type markers in cardiac single-cell clusters, along with interaction networks from the IntAct protein–protein interaction database, are shown in Supplementary Fig. 13a,b (ref. 26).

Across datasets, *SERPINE1* was mainly expressed in fibroblasts, ventricular cardiomyocytes, smooth muscle cells (cluster 3) and endothelial cells (cluster 6). *IL7R* appeared in lymphoid and myeloid cells, smooth muscle cells, endothelial cells and cardiomyocytes (cluster 1). *ANKRD1* was predominantly expressed in ventricular and atrial cardiomyocytes, and in some myeloid cells (Supplementary Figs. 11–13).

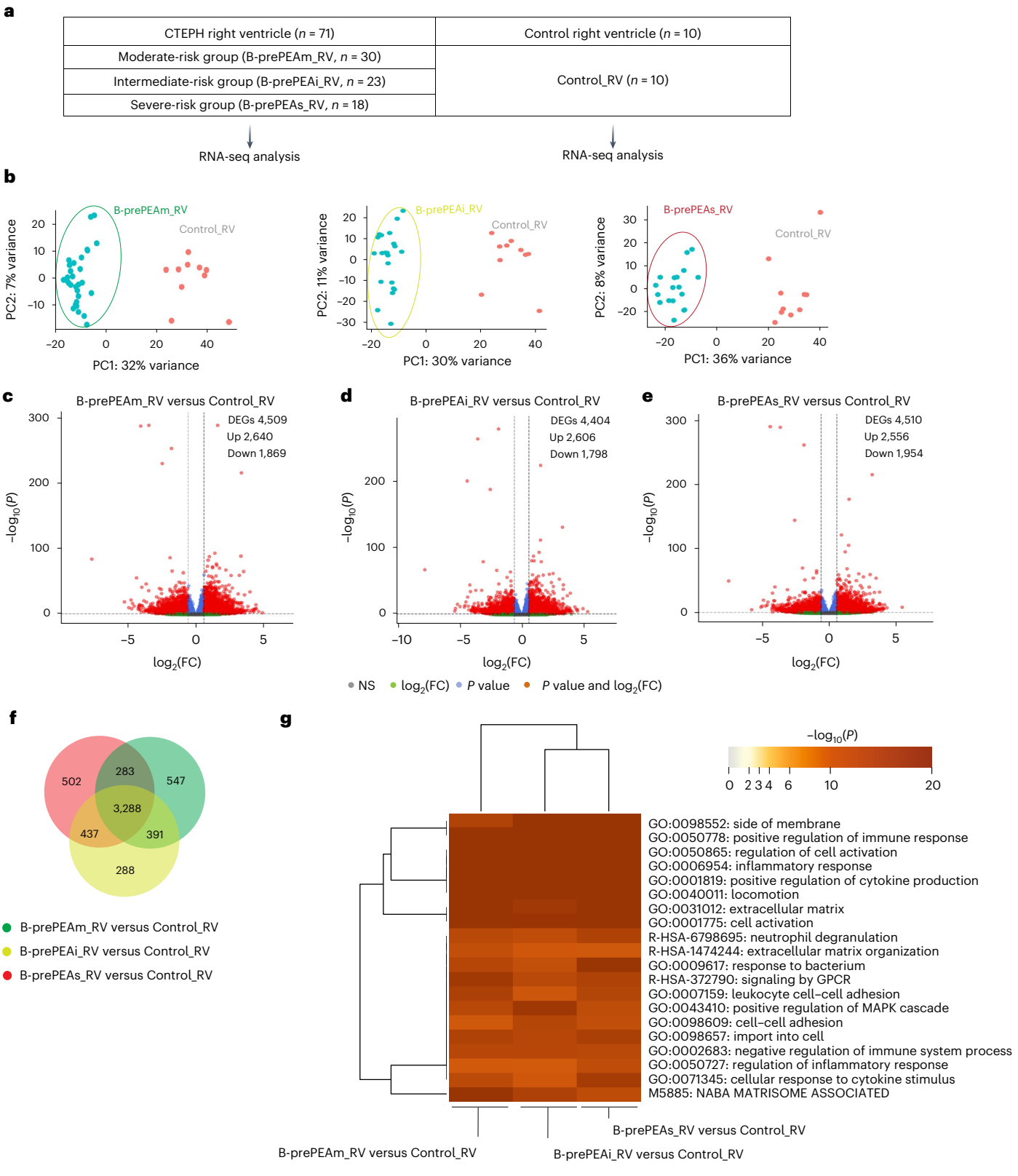

https://doi.org/10.1038/s44161-025-00672-8

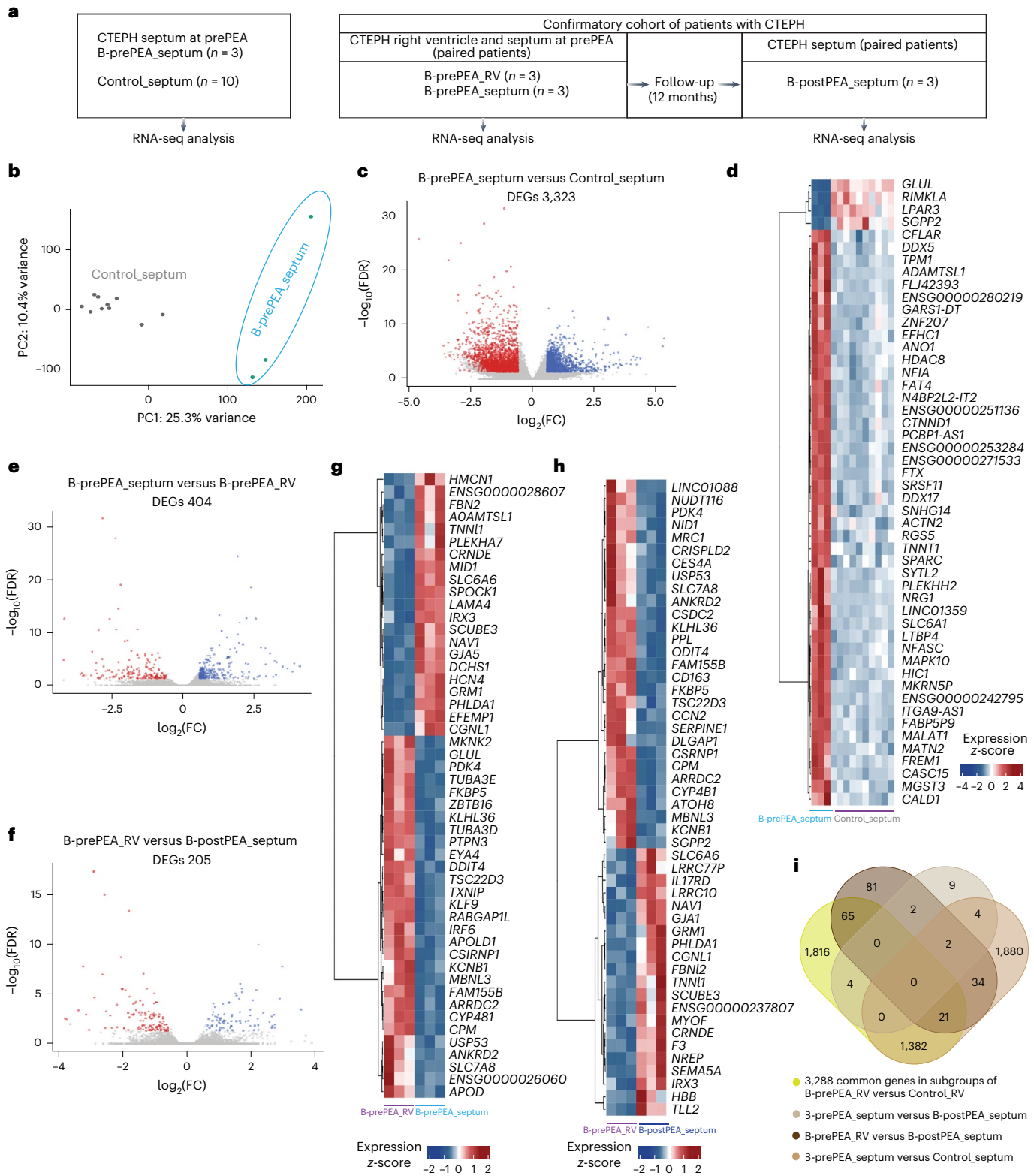

Fig. 4 | Analysis of the transcriptomic profile of the septum before PEA and comparing it with the control septum and after PEA. a, In the confirmatory cohort, RNA-seq analysis was performed on the septum of patients with CTEPH before PEA (B-prePEA_septum, $n = 3$) and the control septum (Control_septum, $n = 10$). Furthermore, RV biopsies were obtained before PEA (B-prePEA_RV, $n = 3$) and septum biopsies (B-postPEA_septum, $n = 3$) 12 months after PEA from the same patients. **b**, PCA plot illustrating the septum before PEA (B-prePEA_septum) and the control septum (Control_septum). **c**, Volcano plot showing significant DEGs (base mean ≥ 5; $|\log_2(FC)| \geq 0.585$; FDR ≤ 0.05) in the B-prePEA_septum (red) versus the Control_septum (blue). **d**, Heatmap showing the top 50 significant DEGs in B-prePEA_septum versus Control_septum. The scaled *z*-score of normalized counts is shown. **e**,**f**, Volcano plot showing the significant DEGs (base mean ≥ 5; $|\log_2(FC)| \geq 0.585$; FDR ≤ 0.05) in B-prePEA_septum (red) versus B-prePEA_RV (blue) (**e**) and B-prePEA_RV (red) versus B-postPEA_septum (blue) (**f**). **g**,**h**, Heatmap showing the top 50 significant DEGs in B-prePEA_septum versus B-prePEA_RV (**g**) and B-prePEA_RV versus B-postPEA_septum (**h**). The scaled *z*-score of normalized counts is shown. **i**, Venn diagram illustrating the common and unique DEGs between the four groups (B-prePEA_RV versus Control_RV, B-prePEA_septum versus B-postPEA_septum, B-prePEA_RV versus B-postPEA_septum and B-prePEA_septum versus Control_septum).

https://doi.org/10.1038/s44161-025-00672-8

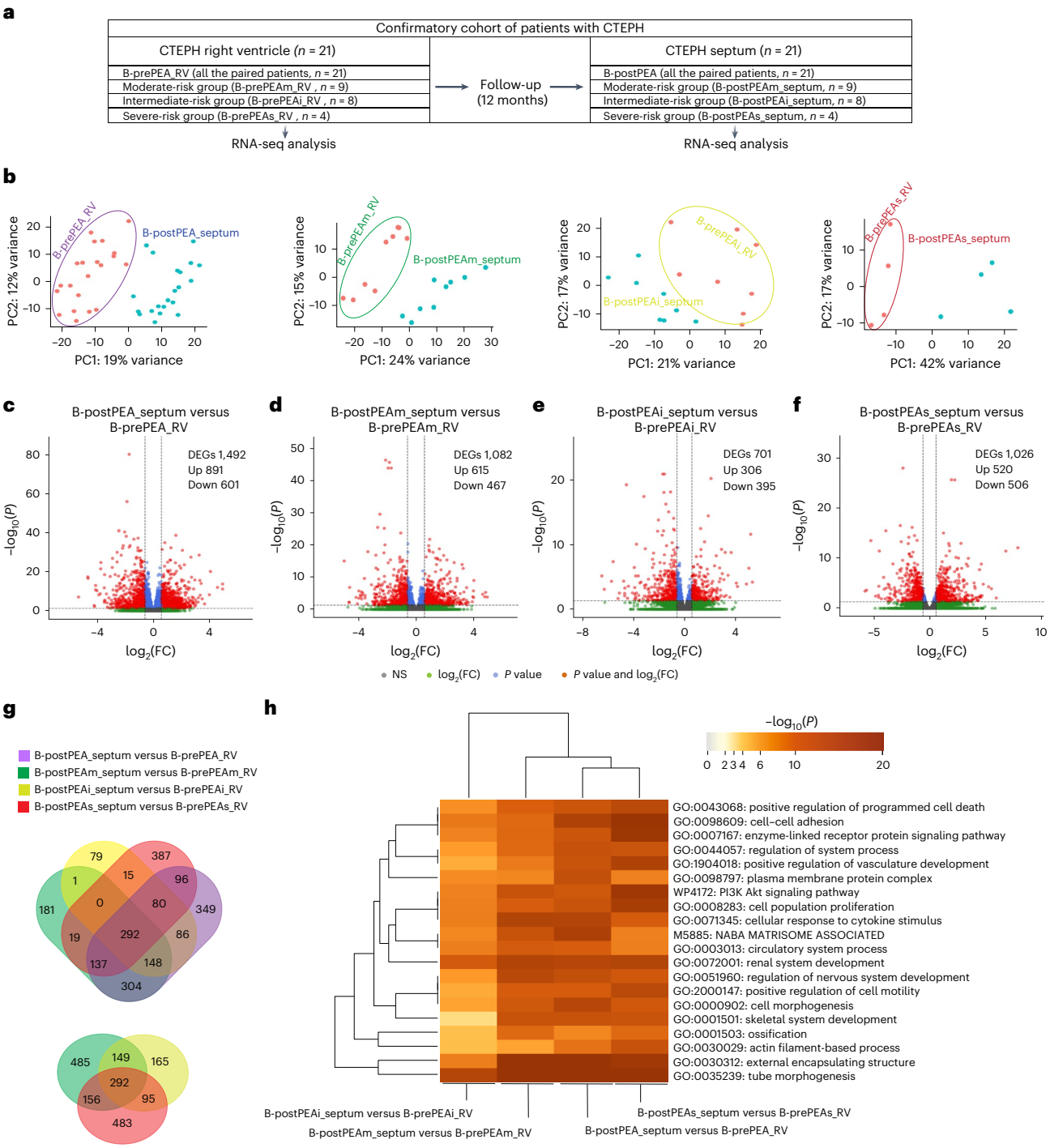

Fig. 5 | Comparing the transcriptomic profiling of the right ventricle and septum in the confirmatory cohort of patients with CTEPH before and after PEA. a, In the confirmatory cohort, gene expression profiles of paired B-prePEA_RV and B-postPEA_septum samples were compared. RNA-seq analysis was performed on 21 RV and septum tissues of patients with CTEPH. Patients at prePEA were categorized into moderate-risk (B-prePEAm_RV, $n = 9$), intermediate-risk (B-prePEAi_RV, $n = 8$) and severe-risk (B-prePEAs_RV, $n = 4$) groups based on their clinical parameters and ESC/ERS guidelines. After 12 months, postPEA_septum biopsies were obtained from the septum tissues of the same patients, including B-postPEAm_septum ($n = 9$), B-postPEAi_septum ($n = 8$) and B-postPEAs_septum ($n = 4$). **b**, PCA plots depicting the RV and septum transcriptomic profiles of patient-paired samples in the following groups: B-prePEA_RV ($n = 21$) and B-postPEA_septum ($n = 21$), B-prePEAm_RV ($n = 9$) and B-postPEAm_septum ($n = 9$), B-prePEAi_RV ($n = 8$) and B-postPEAi_septum ($n = 8$), and B-prePEAs_RV ($n = 4$) and B-postPEAs_septum ($n = 4$). The encircled red dots represent the distinct status of the right ventricle, while the corresponding septum is shown using blue dots. **c**–**f**, Volcano plots showing the distribution of each gene in B-postPEA_septum versus B-prePEA_RV (**c**), B-postPEAm_septum versus B-prePEAm_RV (**d**), B-postPEAi_septum versus B-prePEAi_RV (**e**) and B-postPEAs_septum versus B-prePEAs_RV (**f**). The significant DEGs (base mean expression ≥ 5; $|\log_2(FC)| \geq 0.585$; $P_{adj} \leq 0.05$, two sided) were classified based on $P < 0.05$ and $|\log_2(FC)| > 0.585$ (red dots), only P value (blue dots), $\log_2(FC)$ (green dots) and not significant (gray dots). **g**, Top: Venn diagram illustrating the shared and distinct DEGs in four sets as follows: B-postPEA_septum versus B-prePEA_RV, B-postPEAm_septum versus B-prePEAm_RV, B-postPEAi_septum versus B-prePEAi_RV, and B-postPEAs_septum versus B-prePEAs_RV. Bottom: the common and distinct DEGs among three groups—B-postPEAm_septum and B-prePEAm_RV, B-postPEAi_septum and B-prePEAi_RV, and B-postPEAs_septum and B-prePEAs_RV—are highlighted. **h**, Heatmap illustrating the top 20 overrepresented clusters of terms for all the DEGs between several comparisons: B-postPEAi_septum versus B-prePEAi_RV, B-postPEAm_septum versus B-prePEAm_RV, B-postPEA_septum versus B-prePEA_RV, and B-postPEAs_septum versus B-prePEAs_RV.

To confirm localization and upregulation, immunofluorescence staining was performed on RV tissue from patients with CTEPH in the B-prePEAm_RV and B-prePEAs_RV subgroups. On the basis of atlas data, RV samples were double stained for SERPINE1 and collagen type I alpha 1 chain (COL1A1), IL7R and alpha-smooth muscle actin (αSMA), ANKRD1 and cardiac troponin T (cTNT). Increased staining intensity and co-localization of SERPINE1 in fibroblasts, IL7R in smooth muscle cells and ANKRD1 in cardiomyocytes were observed in B-prePEAs_RV compared with B-prePEAm_RV (Fig. 6d).

To investigate what induces *SERPINE1*, *IL7R* and *ANKRD1*, primary cardiac cells were stimulated with TGF-β1, tumor necrosis factor (TNF) or hypoxia—factors relevant to compensated and decompensated RV states[7] (Supplementary Figs. 14 and 15). In human cardiac fibroblasts (HCFs), *SERPINE1* and *ANKRD1* mRNA were significantly upregulated by TGF-β1 and TNF, while *IL7R* increased with TNF (Supplementary Fig. 14a). In human cardiac microvascular endothelial cells (HCMECs), *IL7R* was significantly increased by TNF, and all three genes were more highly expressed with TNF versus serum stimulation (Supplementary Fig. 14b). Under hypoxia, only *ANKRD1* showed increased expression in HCMECs after 24 h and 48 h compared with normoxia (Supplementary Fig. 15a,b).

To validate these findings in vivo, SERPINE1, IL7R and ANKRD1 expression was examined in two RV dysfunction models: monocrotaline (MCT) and PAB. Hemodynamic and echocardiographic measurements confirmed progressive RV dysfunction at 2, 3 and 5 weeks post-MCT treatment (Extended Data Fig. 9a–c) and at 35 days and 53 days post-PAB (Extended Data Fig. 9d–f). In MCT rats, *Serpine1*, *Il7r* and *Ankrd1* mRNA was significantly elevated at week 5 (Extended Data Fig. 9g–i). In PAB rats, *Serpine1*, *Il7r* and *Ankrd1* were increased (not significantly) (Extended Data Fig. 9j–l). *Serpine1* expression correlated with right ventricular ejection fraction (RVEF) and the ratio of RV mass to the combined LV and septal mass (RV/LV + S) in both models (Supplementary Fig. 16a). *Il7r* expression correlated with RVEF in MCT rats and right ventricular systolic pressure (RVSP) in PAB models (Supplementary Fig. 16b). *Ankrd1* expression correlated with RVSP, RVEF and RV/LV + S in both models (Supplementary Fig. 16c). Together, these findings suggest that *Serpine1*, *Il7r* and *Ankrd1* are key genes in RV remodeling. The downregulation of *Ankrd1* in de-banding mouse models further supports its regulation by pressure unloading.

ANKRD1, SERPINE1 and IL7R regulate cardiac remodeling in vitro

In vitro studies were performed on HCFs and HCMECs using transient transfection of small interfering RNA (siRNA) SMARTpool to investigate the functional role of ANKRD1, SERPINE1 and IL7R in modulating migration, tube formation and cell proliferation. As shown in Supplementary Fig. 17a,b, siRNAs targeting *ANKRD1*, *SERPINE1* and *IL7R* lead to a significant knockdown of the expression of the target genes in HCFs and HCMECs. As *SERPINE1* and *ANKRD1* are the major targets of SMAD/YAP/TAZ target genes[27], the double knockdown of *ANKRD1* and *SERPINE1* suggests that *SERPINE1* and *ANKRD1* have extensive cross-talk in cardiac cells, especially with the greater effect of double knockout of both *SERPINE1* and *ANKRD1* (Supplementary Fig. 18a,b). The number of junctions, total tube length, total mesh area and total segment length were significantly reduced in cells transfected with *siANKRD1* compared with *siCONTROL* in HCMECs (Fig. 7a and Supplementary Fig. 19a). Notably, the effect on migration, that is, the percentage of wound closure, was significantly reduced in *siSERPINE1* and *siIL7R* compared with that in *siCONTROL* (Fig. 7b). In addition, single knockdown of *IL7R*, *ANKRD1* and *SERPINE1* and double knockdown of *ANKRD1* and *SERPINE1* significantly reduced the proliferation of HCFs and HCMECs (Fig. 7c and Supplementary Fig. 19b,c).

Discussion

Characterization of RNA profiles from fresh biopsies of the RV free wall and septum of patients with CTEPH and assessment of the dynamics of these profiles in relation to disease severity and in response to PEA provided valuable information on the RV remodeling and reverse remodeling mechanism in CTEPH. The following are the most important results: first, similar to hemodynamics, RV imaging and biomarkers such as natriuretic peptides, RV free wall RNA profiles differ substantially between patients with CTEPH and controls and between moderate- and severe-CTEPH-risk groups. Second, the RV free wall transcriptomic profiles obtained in a smaller exploratory cohort were validated in a larger confirmatory cohort, providing a solid basis for future use of RNA profiling for in-depth characterization of RV function in patients with PH. Third, histological and molecular analyses of septal tissue show that the RV free wall remodeling is accompanied by extensive septal remodeling, with 40–45% overlap of transcriptomic changes. At both sites, myocyte cytoskeletal changes are accompanied by major matrisomal changes in intermediate- and severe-risk groups. Fourth, intraindividual comparison of histological and gene expression profiles (septal to septal comparison or free wall comparison to the overlapping septal transcriptome) before and after PEA shows far-reaching reversal of the myocyte cytoskeletal and matrisomal changes. Similarly, reversal of transcriptomic changes was partly found in an experimental PA banding and de-banding model. Fifth, various signaling molecules and pathways were identified (ANKRD1, IL7R, SERPINE1), correlating with disease severity (hemodynamics, RV function) and reverse remodeling, putatively offering for RV-focused preventive or therapeutic strategies (Extended Data Fig. 10).

The current PH guidelines recommend a multidimensional diagnostic approach for individual risk stratification. Calculating risk scores from the three-strata ESC and ERS risk stratification model using parameters focused on the right heart (CI, TAPSE/sPAP and natriuretic peptides) for the CTEPH cohorts allowed us to define patients at moderate, intermediate or severe risk[8]. Similar to other CTEPH cohorts, patients in our study had markedly impaired pulmonary hemodynamics associated with elevated natriuretic peptides[11,28]. In addition to the functional status of the right ventricle, patients also differed from controls in terms of transcriptional characteristics of the RV free wall, indicating molecular, cellular and structural changes underlying the development of functional RV phenotypes. Importantly, the transcriptomic profiles of the RV free wall obtained in a smaller exploratory cohort were validated in a larger confirmatory cohort,

Fig. 6 | Expression levels of *SERPINE1*, *IL7R* and *ANKRD1* in the right ventricle and septum, and their correlation with the clinical parameters of the confirmatory cohort of patients with CTEPH. a, The mRNA expression levels (normalized read counts) of *SERPINE1* in CTEPH right ventricle at prePEA (B-prePEAm_RV, $n = 30$; B-prePEAi_RV, $n = 23$; B-prePEAs_RV, $n = 18$) and the mRNA expression levels of *SERPINE1*, *ANKRD1* and *IL7R* before PEA (B-prePEA_RV, $n = 21$) and after PEA (B-postPEA_septum, $n = 21$) in the confirmatory cohort of patients with CTEPH are shown. Data are presented as mean ± SEM, and *P* values were calculated using one-way ANOVA followed by Tukey's multiple-comparison tests for expression of *SERPINE1* at prePEA and using a Wilcoxon test for the prePEA versus postPEA comparison. The boxes show the IQR (25th to 75th percentile), and the central bands indicate the median. The whiskers extend to 1.5 times the IQR above and below the box. **b**,**c**, The correlation between rlog(read counts) of *SERPINE1* (**b**) and *ANKRD1* (**c**), with clinical parameters of the patients before PEA (B-prePEAm_RV, B-prePEAi_RV and B-prePEAs_RV) is shown. Pearson's correlation coefficient (*r*) and its associated two-tailed *P* value are shown in each graph. **d**, Representative immunofluorescent images of the right ventricle from the confirmatory cohort of patients with CTEPH before PEA are shown. The RV tissues from B-prePEAm_RV and B-prePEAs_RV patients underwent dual staining with SERPINE1 and COL1A1 (B-prePEAm_RV, $n = 4$, and B-prePEAs_RV, $n = 3$), IL7R and α-SMA (B-prePEAm_RV, $n = 4$, and B-prePEAs_RV, $n = 3$) and ANKRD1 and cTnT (B-prePEAm_RV, $n = 4$, and B-prePEAs_RV, $n = 4$) antibodies. Scale bars, 50 µm.

https://doi.org/10.1038/s44161-025-00672-8

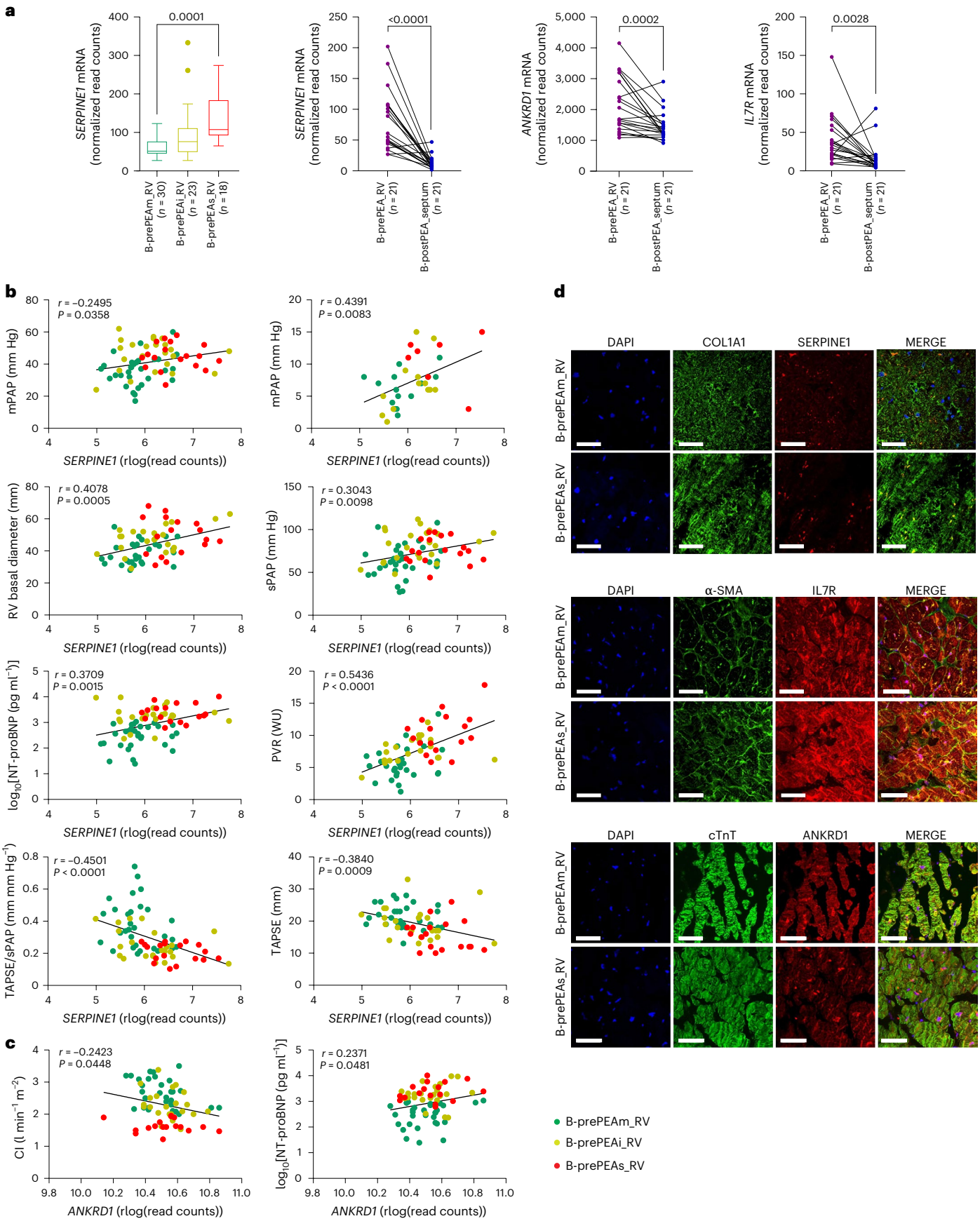

https://doi.org/10.1038/s44161-025-00672-8

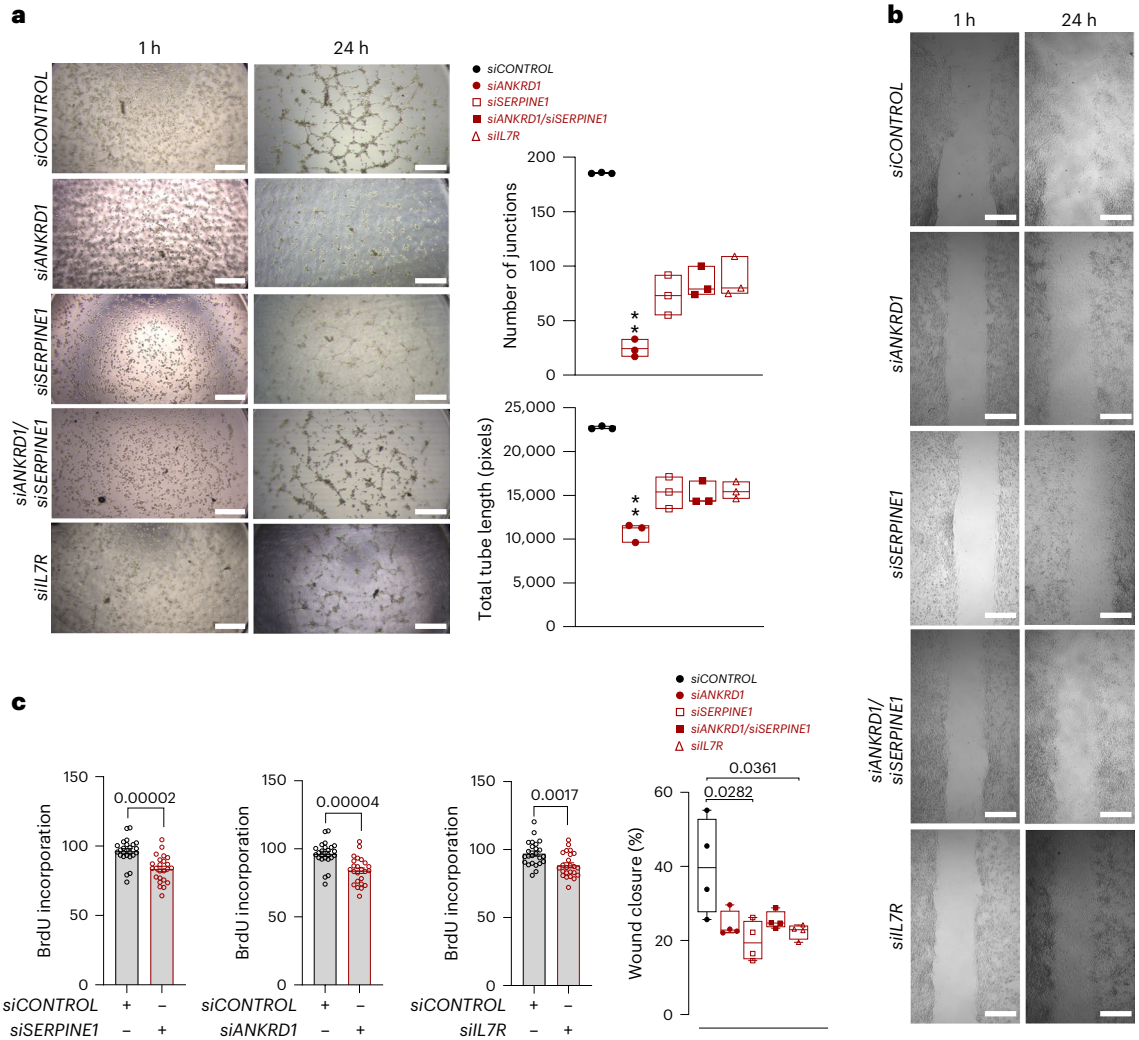

Fig. 7 | Inhibition of *SERPINE1*, *IL7R* and *ANKRD1* in HCFs and HCMECs. **a**, HCMECs were transfected with siRNA for 48 h, followed by a 24 h tube formation assay. The representative images were taken at 1 h and 24 h. The number of junctions and total tube length were analyzed and quantified using ImageJ software. Data are presented as mean ± SEM. ($n = 3$ biological replicates; Kruskal–Wallis test, $^{**}P = 0.0021$ compared with scrambled siRNA). Scale bars, 1 mm. The boxes show the IQR (25th to 75th percentile), and the central bands indicate the median. The whiskers extend to 1.5 times the IQR above and below the box. **b**, HCFs were transfected with siRNA for 48 h, followed by a 24 h tube migration assay. Representative images were taken at 1 h and 24 h, and the percentage of wound closure was analyzed and quantified using ImageJ software with the wound healing analyzer plugin. A scrambled siRNA pool was used as a negative control. The data are presented as mean ± SEM. ($n = 3$ biological replicates with only one having one technical replicate; two-tailed unpaired *t*-test). Scale bars, 1 mm. The boxes show the IQR (25th to 75th percentile), and the central bands indicate the median. The whiskers extend to 1.5 times the IQR above and below the box. **c**, HCFs were transfected with siRNA for 48 h, and the proliferation was measured using BrdU incorporation assay. Data are presented as mean ± SEM. ($n = 4$ biological replicates and 6 technical replicates; two-tailed unpaired *t*-test). Black empty circles represent cells transfected with siCONTROL, and red empty circles represent cells transfected with target siRNA.

providing a solid foundation for the future use of RNA profiling for in-depth characterization of RV function in PH patients.

Comparison of the RNA profiles in the different risk classes in both the exploratory and confirmatory cohorts to normal RV control tissue revealed enrichment of various GO terms such as enzyme–receptor–protein signaling pathway, cytoskeleton, cell adhesion molecule binding, NABA MATRISOME ASSOCIATED and adipogenesis. These transcriptomic changes increased with risk class severity, and in particular, changes in highly regulated ECM-related genes were found to be correlated with indicators of disease severity such as RV basal diameter, mean right arterial pressure (mRAP), CI, PVR, mPAP, NT-proBNP, sPAP and TAPSE/sPAP. In companion with the increased fibrotic changes in the histologic sections of free RV wall biopsies, these findings are well in line with previous studies, documenting increased fibrosis in cardiac tissue originating from patients with idiopathic PAH or CTEPH[29]. This fibrotic remodeling observed in the CTEPH high-risk group might represent a maladaptive response, linked with increased diastolic stiffness, disrupted cardiomyocyte excitation–contraction coupling and impaired myocardial contraction coordination[30,31].

Adipogenesis was consistently enriched in intermediate- and severe-risk groups in both cohorts. This aligns with findings that increased epicardial adipose tissue volume is associated with RV end-diastolic volume and NT-proBNP in PAH, and linked to reduced long-term event-free survival in patients with PAH[32]. Similarly, lipid accumulation and fatty acid metabolism alterations have been reported in the right ventricle of patients with PAH[33,34]. While the role of adipose tissue and lipotoxicity in maladaptive RV remodeling is not fully understood, their impact on diastolic function and profibrotic signaling—such as TGF-β activation—should be considered[35].

GO terms related to inflammation—such as regulation of inflammatory response, cytokine signaling and neutrophil degranulation—were enriched in CTEPH RV tissue compared with controls, increasing with

disease severity. This indicates progressive inflammatory changes in the right ventricle. RV inflammation has previously been reported in various PH forms, including acute pulmonary embolism and HIV-associated, systemic-sclerosis-associated and idiopathic PAH[7,30,36]. Although not directly studied in CTEPH, RNA-seq data from decompensated PAH right ventricles showed increased inflammatory gene signatures, with elevated $CD68^+$ macrophages and IL-1β levels, compared with controls[7,30]. These findings, together with our current data, suggest that inflammation is a key contributor to adverse RV remodeling under chronic pressure overload in CTEPH[36].

In summary, a sequence of transcriptomic, cardiomyocyte-phenotypic and matrisomal changes appear to underlie the transition from an adaptive to a maladaptive response of the right ventricle under CTEPH conditions. For the selection of therapeutic targets specifically focusing on these RV sequence of events, it is of interest that only 10–40% of the RV transcriptomic changes overlap with transcriptomic changes reported to underlie left ventricular failure[20,22]. Whether these results can be extrapolated to PH groups other than CTEPH requires further integrated bioinformatic and clinical correlation analyses in non-CTEPH cohorts. Previous studies from our and other groups[6,7] in RV-omics in PH suggest that despite some common regulatory pathways (for example, signaling cascades related to ECM, cell cycle, energy metabolism and inflammation) in different PH groups, distinct and uniquely enriched pathways (for example, epithelial–mesenchymal transition in right ventricles in PAH, increased oxidative stress in right ventricles in CTEPH) may exist, which require further in-depth investigation.

Although changes in septal thickness and motion, correlating with RV afterload, are well known for PH constellations including CTEPH[37,38], there are only scarce data on detailed histological and molecular profiling of septal biopsies under these conditions. We observed septal histomorphological (cardiomyocyte hypertrophy and increased fibrosis) changes largely corresponding to those in the free RV wall, as well as enrichment of GO terms associated with cytoskeletal changes of the cardiomyocytes and the ECM. Interestingly, however, the transcriptomic profiles of the remodeled septum overlaid not fully, but around 40–45%, with the transcriptome of the remodeled RV free wall. Septal remodeling may thus have some specific features, possibly related to its origin of both first and second heart fields[39], whereas the RV free wall originates from the second heart field, or to its positioning between the right and the left ventricle, receiving biomechanical forces from both sides.

The therapy of choice in patients with CTEPH is surgical PEA. For inoperable patients, an interventional balloon pulmonary angioplasty is recommended[9]. Both therapies improve pulmonary hemodynamics and allow right heart recovery, which is illustrated by invasive hemodynamic measurements, imaging findings and biomarker dynamics. Comparable to other cohorts, the patients with CTEPH in our study showed markedly improved pulmonary hemodynamics, decreased natriuretic peptides and an improved right heart function after therapy[28,40–47]. Our study, however, performs an intraindividual comparison of heart biopsies before and after PEA in these patients with CTEPH. This approach shows a reduction in hypertrophy and fibrosis and an improvement in vascularization relative to RV myocardial tissue volume in response to the afterload relief, correlating with improved clinical parameters (RV basal diameter, TAPSE/sPAP and PVR) 12 months after PEA. A comparison of RNA profiles between RV free wall and septal biopsies before and after PEA, focusing on overlapping transcriptomic changes between these two sites, revealed alterations of terms related to muscle contraction, cytoskeleton changes and ECM, corresponding to most of the pathways that were markedly altered in intermediate- and severe-risk patients with CTEPH, suggesting reverse remodeling of the RV septal molecular, cellular and structural changes in response to PEA. However, residual myocardial fibrosis in septal biopsies and the identification of GO terms associated with ECM changes in patients with CTEPH 12 months after PEA suggest still incomplete reversal of fibrosis. A comparison of these human reverse-remodeling gene expression datasets with the RV tissue gene arrays of the PA banding–de-banding mouse model[23] unexpectedly shows only 10% overlap between the human and the mouse system. Imperfect mimicry of the CTEPH and PEA constellation by the banding and de-banding procedure, differences in observation periods and species specificities might explain these differences. However, reversal of the afterload-induced RV transcriptomic changes was also shown in the mouse model.

Three DEGs associated with reverse remodeling—*ANKRD1/CARP*, *SERPINE1* and *IL7R*—showed significant correlations between B-postPEA_septum and B-prePEA_RV expression levels and patient hemodynamics. Public databases (human cardiac cell atlas, heart atlas, protein atlas) and double immunofluorescence staining linked SERPINE1 to fibroblasts, IL7R to smooth muscle cells and ANKRD1 to cardiomyocytes. Experimental data suggest roles in cell proliferation, migration, wound healing and angiogenesis. These genes were upregulated by hypertrophic stimuli and pathways associated with decompensated right ventricles, such as TNF and TGF-β (ref. 7). ANKRD1 expression has been linked to reduced contractility and compliance in end-stage heart failure[48] and modulates remodeling via the ERK/GATA4 pathway[49,50]. SERPINE1/PAI-1 may either repress fibrosis or promote ECM accumulation and scarring[51]. IL7R upregulation suggests inflammatory cell recruitment and chemokine expression in maladaptive right ventricles. Further studies are needed to clarify their roles in RV failure and recovery under CTEPH and PEA conditions.

Taken together, comprehensive transcriptomic profiles from RV and septal biopsies of living patients with CTEPH not only provide valuable information on the molecular mechanisms underlying RV and septal remodeling during increased afterload and its reversibility upon unloading, but also offer targets for therapeutic intervention.

Limitations

In this study, RNA-seq analysis was performed in patients with CTEPH undergoing PEA. However, the small number of consecutively enrolled patients in the study cohort was a limitation that needed to be considered. However, the data were sufficient to show considerable differences in RNA profiles between moderate- and severe-risk patients with CTEPH and could be validated in a second confirmatory cohort. This study used a right-heart-focused risk stratification model adapted from the ESC/ERS guidelines for PH. This model has not yet been validated in a clinical outcome study. However, all recommended diagnostic aspects (hemodynamics, biomarkers, imaging) of the right heart examination were considered. Furthermore, as a human model of RV remodeling and reverse remodeling after PEA, CTEPH provides an ideal intra-observation opportunity compared with other datasets derived from transplanted hearts. Despite the different locations of biopsies between the RV free wall and septum, the timing of the biopsy removal and the effect of the surgical procedure, our data clearly show several overlaps between the RV wall and septum, emphasizing the relevance of the results.

Additional limitations of the study lie in the animal models used to validate the transcriptome results of a few genes (*SERPINE1*, *IL7R* and *ANKRD1*). We used RV tissues from the MCT and PAB models. Although we expect the same changes in the in vivo CTEPH model, the question of whether the molecular changes are mainly caused by pressure unloading remains to be validated in the in vivo CTEPH model. Although we have confirmed the regulation of some genes at the protein level, not all RNA changes can be translated into changes in protein expression, so a proteomic study of this valuable human cohort is warranted. As the in vitro experiments were performed on cardiac cells from the LV and the LV and right ventricle are developmentally distinct, additional experiments with cells isolated from the right ventricle are important.

Methods

Ethics in human studies

The study of CTEPH cohorts was approved by the ethics board of the Justus Liebig University of Giessen (AZ 44/14, 144/11, 145/11, 146/11, 199/15) and is in accordance with the declaration of Helsinki, and all the patients with CTEPH enrolled in the study gave written informed consent. For the healthy control participants, all experimental procedures were conducted in accordance with the ethical standards of the responsible institutional and national committee on human experimentation, as outlined in the Helsinki Declaration (1975). Written informed consent was obtained from all control participants involved in the study according to the protocol approved by the Local Ethics Committees of the National Institute of Cardiology, Warsaw, Poland (approval number: IK-NPIA-0021-14/1426/18).

Ethics in animal studies

All the animal experiments were conducted in accordance with the National Institute of Health Guidelines on the Use of Laboratory Animals. The study protocols were approved by the University Animal Care Committee and the Federal Authorities for Animal Research of the Regierungspräsidium Giessen (GI 20/10 Nr G92/2017 RP Giessen), Hessen, Germany.

Patient cohorts and clinical assessment

This study included 96 patients with CTEPH, who were treated by PEA at the Kerckhoff Heart and Thorax Centre between 2016 and 2020. The standard periprocedural management of such patients was recently published[40]. In brief, clinical examination, echocardiography, 12-lead electrocardiogram, laboratory tests, 6-min walk test, ventilation–perfusion scan, computed tomography angiography, right-heart catheterization (RHC) and pulmonary angiography were assessed for all patients before PEA (prePEA). The final diagnosis of CTEPH was made according to the guidelines in symptomatic patients after 3 months of effective anticoagulation, with an mPAP ≥ 25 mm Hg at rest and typical obstructive pulmonary vascular lesions on imaging diagnostics[52]. All patients were presented in an interdisciplinary CTEPH conference to define the therapeutic concept and approved feasibility for surgical PEA as the first-line therapy. Routinely, a standardized follow-up assessment of patients was performed 12 months after PEA (postPEA).

PEA

The performance of PEA was conducted according to the standardized procedure[40]. In brief, a median sternotomy was followed by the connection of patients to the heart–lung machine for extracorporeal circulation, with subsequent cooling to a core temperature of 18 °C. PEA was performed in repetitive phases of deep hypothermic circulatory arrest to avoid collateral blood backflow from systemic arteries and to optimize visualization. The removal of scar tissue from the pulmonary vasculature was accomplished by creating an endarterectomy plane between the intima and media of the vessel wall, with the aim of achieving complete excision. Following the endarterectomy, patients were rewarmed and weaned from bypass at a body temperature of 36 °C. The standard postoperative care includes a stay at the intensive care unit for another 2 days, extubation on the second postoperative day and discharge after 12 days (ref. 40).

RHC

As a component of the diagnostic protocol, patients underwent RHC at before PEA and 12 months after PEA. The RHC was routinely performed via the right internal jugular vein using a 6-F sheath and a standard Swan–Ganz catheter. The medication of the patients was not modified before or during RHC; in particular, no vasoactive agents were administered.

Human RV and septum acquisition and classification of patients with CTEPH

This prospective study enrolled a total of 96 patients with CTEPH, divided into two distinct cohorts: an exploratory cohort and a confirmatory cohort. RV biopsies were obtained from the right ventricular free wall of the patients who underwent the PEA procedure (prePEA_RV) from two cohorts: the exploratory cohort (A-prePEA_RV, $n = 14$) and the confirmatory cohort (B-prePEA_RV, $n = 88$). The patients in each cohort were risk stratified based on their clinical parameters and ESC/ERS guidelines using a three-strata model into moderate-, intermediate- and severe-risk groups[8]. In addition, the study included 26 postPEA septum biopsies collected 12 months after PEA, and 21 were matched with prePEA counterparts. In addition, in the confirmatory cohort, in the subgroup of 3 patients, with the biopsies before PEA from the right ventricle (B-prePEA_RV, $n = 3$) and 12 months after PEA from the septum (B-postPEA_septum, $n = 3$), the biopsy was obtained from the septum before PEA (B-prePEA_septum, $n = 3$). The clinical parameters of all the patients with CTEPH are shown in Table 1 and Supplementary Tables 1–6. All the specimens were processed in a standardized manner by experienced staff, who were blinded to clinical data. Out of 88 RV biopsy samples, RNA-seq was performed on 71 samples and histological analysis on 43 samples, with 26 samples overlapping between the two datasets. The allocation to RNA-seq or histology was not based on any pre-selection, bias, or stratification criteria, but rather determined solely by the amount of tissue available from each biopsy.

Tissue samples from healthy control participants were collected from the same patient ($n = 10$) for both the right ventricle and septum. The tissue samples for control were collected in the Department of Heart Failure and Transplantology, National Institute of Cardiology, Warsaw, Poland. Healthy human hearts were obtained from organ donor patients (control, $n = 10$) whose hearts were not used for transplantation owing to technical reasons (for example, donor and recipient incompatibility). The donors did not have any relevant previous cardiological history or any abnormalities in electrocardiography and echocardiography (LV dimensions and contractility within normal ranges). The tissue samples from the ventricular free wall were taken (avoiding scarred, fibrotic or adipose tissue, endocardium, epicardium or coronary vessels).

Total RNA extraction from human heart tissue

We used two distinct RNA extraction methods to isolate the total RNA of human heart tissue of patients with CTEPH. In the bead beating homogenization method, tissue homogenization was performed using a BeadBug 3 homogenizer (Biozym). Subsequently, RNA isolation was performed using a miRNeasy Micro Kit (Qiagen, 217084) according to the manufacturer's instructions. RNA isolation was performed using this method on the RV tissue of the exploratory cohort of patients with CTEPH (A-prePEA_RV, $n = 14$).

The dry cryopulverization method was performed to isolate the RNA from the right ventricle and septum tissue from the confirmatory cohort of patients with CTEPH including B-prePEA_RV ($n = 71$), and septum tissue of B-postPEA_septum ($n = 21$) and B-prePEA_septum ($n = 3$). The biopsy samples were transferred to pre-chilled TT05 culture tubes and processed using a CP02 cryoPREP Automated Dry Pulverizer 110 V (Covaris). The remaining RNA isolation steps were performed using the miRNeasy Micro Kit (Qiagen, 217084) according to the manufacturer's protocol. Total RNA was extracted from the right ventricle and septum of the healthy control participants, using the RNeasy PowerLyzer Tissue & Cells Kit (Qiagen) according to the manufacturer's instructions outlined in the RNeasy handbook. To prevent genomic DNA contamination, isolated RNA was treated with on-column DNase digestion (DNase-Free DNase Set, Qiagen).

Library preparation and RNA sequencing data analysis

RNA and library preparation integrity were verified with LabChip Gx Touch 24 (Perkin Elmer). For library preparation, approximately 100 ng

to 1 µg of total RNA was used as input for the SMARTer Stranded Total RNA Sample Prep Kit - HI Mammalian (Takara Bio). Sequencing was performed on a NextSeq 2000 (Illumina) using P2 flow cell with v3 chemistry with 1 × 72 bp single-end setup or NextSeq500 (Illumina) using v2 chemistry with 1 × 75 bp single-end setup. The resulting raw reads were assessed for quality, adapter content and duplication rates with FastQC[53]. Trimmomatic version 0.39 was applied to trim reads after a quality drop below a mean of Q15 and Q18 in a window of five nucleotides. Afterward, only filtered reads longer than 15 nucleotides were kept[54]. Only reads above 30 nucleotides were cleared for further analyses. The reads were aligned versus Ensembl human genome version hg38 using Ensembl release 101 for the control cohort and release 104 for the CTEPH cohorts. The alignment was performed with STAR, using version 2.7.9a for the control cohort and version 2.7.10a for the CTEPH cohort. The parameter '--outFilterMismatchNoverLmax 0.1' was set to increase the maximum ratio of mismatches to mapped length to 10% (ref. 55). Aligned reads were filtered to remove duplicates with Picard 2.27.1 (Picard Toolkit, 2019, Broad Institute, GitHub repository, https://broadinstitute.github.io/picard/; Broad Institute; RRID: SCR_006525), multi-mapping, ribosomal or mitochondrial reads. The gene counts were established with the featureCounts 2.0.2 tool from the Subread package[56]. Only reads mapped to the exon and aggregated per gene were included for analysis. The reads with overlapping multiple genes were excluded. DEGs were identified using DESeq2 version 1.30.0 applied to the control cohort and 1.30.1 applied to the CTEPH cohort[57]. Based on the raw count matrix, the contrasts were created with DESeq2.

Downstream analysis of RNA-seq data

Significantly differentially expressed genes were identified using a threshold of mean read count ≥5 and a maximum Benjamini–Hochberg corrected *P* value of ≤0.05, and $|\log_2(FC)| \geq 0.585$. The annotations were enriched with UniProt data based on Ensemble gene identifiers (activities at the Universal Protein Resource (UniProt)). All the downstream analysis was performed based on the normalized gene count matrix. A global clustering heatmap of the samples was generated based on the Euclidean distance of regularized log-transformed gene counts. PCA as a dimension reduction analysis was performed on regularized logarithm-transformed counts using R package[58]. Volcano plots were generated to visualize the DEGs based on DESeq2 normalized counts. For further analysis, R (version 4.2.0) and RStudio (version 2023.03.0, Build 386) were used in conjunction with several specialized R packages including DESeq2 (version 1.38.3) for the differential gene expression analysis, sva (version 3.46.0), ComBat_seq for surrogate variable analysis and batchcorrection[59] and Complexheatmap (version 2.14.0) for Heatmaps[60,61].

Pathway enrichment analyses were conducted using Metascape (www.metascape.org). Pathway and process enrichment analysis was performed with the default settings, using KEGG Pathway, GO Biological Processes, GO Cellular Components, GO Molecular Functions, Reactome Gene Sets, Canonical Pathways, CORUM, WikiPathways, PANTHER Pathway and all genes in the genome as the enrichment background. Terms with a *P* value <0.01, a minimum count of 3 and an enrichment factor >1.5 were collected and clustered based on their membership similarities. *P* values were calculated based on the cumulative hypergeometric distribution, and *q* values were computed using the Benjamini–Hochberg procedure to account for multiple testing. Kappa scores were used as the similarity metric when performing hierarchical clustering on the enriched terms, and sub-trees with a similarity of >0.3 were considered a cluster. The most statistically significant term within a cluster was selected to exemplify the cluster. For multiple gene lists, these were merged into a single list named '_FINAL'. If the terms were enriched in several individual gene lists and/or the _FINAL gene list, the best *P* value was selected as the final *P* value[62].

Statistical analysis

Several tests were used for statistical analysis using GraphPad Prism version 9.1.0 (GraphPad Software). For normally distributed variables, comparison between two groups was performed using unpaired *t*-tests, while paired *t*-tests were used where applicable. Non-normally distributed variables are presented as median (interquartile range (IQR)). The comparison between the two groups was performed using the Mann–Whitney *U*-test, while the Wilcoxon matched-pairs signed-rank test was used for the paired data. For the comparisons involving more than two groups, one-way analysis of variance (ANOVA) was used for the normally distributed variables. For the non-normally distributed variables, the Kruskal–Wallis test was used. In addition, categorical variables are shown as counts and percentages and Fisher's exact test was performed to compare the categorical variables. Pearson's correlation analysis was used to show the relationship between the regularized logarithm transformation (rlog) read counts of the selected genes and the clinical parameters of the patients.

Histopathological, immunohistochemical and immunofluorescence analyses

For investigation of fibrosis and hypertrophy in patients with CTEPH, RV and septum tissue were sectioned into 5-µm-thick slices from embedded paraffin tissue. To assess fibrosis, Sirius red staining was performed, while hematoxylin–eosin (H&E) staining was used to evaluate hypertrophy. To quantify the fibrosis in the right ventricle and septum of patients with CTEPH, the cellSens Standard software version 4.3 (Evident Scientific) was used. For the analysis of fibrotic area fractions, a variable number of sections per patient were analyzed to give a tissue area and the corresponding areas of the region of interest (ROI). Areas were summed up per patient, and the area fraction of the ROI per patient was calculated by dividing the summed areas (ROI area/tissue area). Differences in the area fractions between the different risk groups were analyzed in R 4.1.1 (ref. 63) using a weighted generalized linear model of the quasi-binomial family, using the total tissue areas per patient as weights. The area fractions in the right ventricle and septum were compared using a paired-sample *t*-test on the log fractions, using the total tissue area per patient as weights.

The cross-sectional area of cardiomyocytes was morphometrically assessed using Olympus CellSens Entry 2.3 software by selecting the best-preserved cardiomyocytes with centrally located nuclei, ensuring accurate and reliable measurements.

For the assessment of vascularization, the heart tissue sections were stained according to a standardized protocol (Bond Max staining protocol) using the monoclonal CD34 antibody Novocastra (Liquid Mouse Monoclonal Antibody Endothelial Cell Marker, number NCL-L-END, Leica Biosystems Newcastle). The BOND Polymer Refine Detection system (number DS9800, Leica Biosystems Newcastle) was applied for visualization. The tissue sections were also counterstained with hematoxylin, resulting in endothelial cells appearing brown and cell nuclei appearing blue to violet. Quantification was performed using Olympus CellSens Entry 2.3 software.

For immunofluorescence analysis, RV tissue from subgroups of patients with CTEPH at prePEA including B-prePEAm_RV and B-prePEAs_RV were embedded in OCT and sectioned into 8-µm slices. Tissue sections were washed with PBS before undergoing a 10-min incubation with a permeabilization buffer containing 0.5% Triton X-100 (Carl Roth) at room temperature. Following an additional set of PBS washes, a blocking buffer, PBS supplemented with 5% bovine serum albumin (Carl Roth), was applied and allowed to incubate for 1 h at room temperature. Subsequently, the slides were incubated with two primary antibodies including PAI1 monoclonal antibody (SERPINE1, 1:200, number MA1-40224, Thermo Fisher) and COL1A1 polyclonal antibody (1:500, number PA5-29569, Thermo Fisher), CD127 polyclonal antibody (IL7R, 1:200, number PA5-102399, Thermo Fisher) and alpha-smooth muscle actin antibody (αSMA, 1:2,000, number

NB300-978, Novus), CARP polyclonal antibody (ANKRD1, 1:400, number PA5-101170, Thermo Fisher) and cardiac troponin T monoclonal antibody (13-11) (cTnT, 1:1,000, number MA5-12960, Thermo Fisher) diluted in PBS for co-staining, and incubated overnight at 4 °C. The following day, tissue sections were washed with PBS, and slides were incubated with corresponding secondary antibodies (anti-mouse 594, 1:500, number A21203, Thermo Fisher; anti-rabbit 488, 1:500, number A11008, Thermo Fisher; anti-rabbit 594, 1:500, number A32740, Thermo Fisher; anti-goat 488, 1:500, number A21467, Thermo Fisher; anti-mouse 488, 1:1,000, number A11029, Thermo Fisher) for 1 h at room temperature. Afterward, sections were stained with DAPI (Thermo Scientific) at a dilution of 1:1,000 in PBS, followed by a 10-min incubation and a final set of PBS washes. Ultimately, slides were mounted and covered with coverslips, then stored at 4 °C, or prepared for immediate fluorescent image acquisition with an LSM 710 confocal microscope.

PAB and MCT rat modes

In animal studies, Sprague Dawley male rats (*Rattus norvegicus*) aged 8–10 weeks (PAB group) and 10–12 weeks (MCT group) were obtained from Charles River and subjected to the treatment. PAB rats were anesthetized with a subcutaneous injection of analgesic buprenorphine hydrochloride (Temgesic, 0.1 mg kg^{-1}, Sigma-Aldrich) and maintained with 3–4% isoflurane mixed with oxygen via inhalation. Following intubation, the rats were connected to a ventilator (MiniVent type 845 Hugo Sachs Elektronik), and the respiratory rate and the stork volume were adjusted according to animal weight. The left thoracic wall of the rats was depilated and disinfected with Braunoderm (Braun). A small skin incision was made at the axillary level followed by careful separation of the thoracic muscles to open the chest cavity through a small incision in the second intercostal space. This exposed the pulmonary artery, aorta and left atrium. The pulmonary artery was then carefully separated from the aorta and left atrium, and an L-shaped blunted needle was placed around it, secured tightly against the needle. A titanium ligating clip (Hemoclip, Edward Weck) was placed around the pulmonary artery to produce 65–70% constriction. The chest cavity was then closed, and the muscles were repositioned to their original place. In the sham groups, the pulmonary artery was dissected using an L-shaped needle, but no ligating clip was applied, and the chest cavity was immediately closed.

MCT rats were injected with either a single subcutaneous MCT dose (60 mg kg^{-1} body weight) or an equal volume of saline for the control group.

The hemodynamics measurements were performed after 2, 3 and 5 weeks of MCT injection in rats and, for the PAB rats, on day 35 and 53 after the PAB and sham operation. The hemodynamic parameters include cardiac contrast-enhanced microscopic computed tomography (μCT), RHC and RV hypertrophy measurements as described[64].

Treatment of human cardiac cells

The HCFs were purchased from ScienCell Research Laboratories (catalog number 6300) and cultured on poly-L-lysine-coated dishes in fibroblast medium as recommended by the supplier. HCMECs were purchased from PromoCell (catalog number C-12285) and maintained in Endothelial Cell Basal Medium MV2, supplemented with SupplementPack Endothelial Cell GM MV2. The cells were cultured at 37 °C in a humidified chamber with 5% CO_2. HCF cells and HCMECs were treated with different PH stimuli, including TGFβ1 (10 ng; Peprotech) and TNF (10 ng; Peprotech), for 48 h. For hypoxia (Hox) treatment, HCF cells and HCMECs were maintained in a humidified hypoxia chamber with 5% CO_2 and 1% O_2 at 37 °C for 6, 24 and 48 h. By contrast, the normoxia (Nox) condition was used as a control, and the cells were maintained with the same medium in a cell culture incubator with 5% CO_2 and 21% O_2 at 37 °C.

RNA interference

Transfection of HCF cells and HCMECs was performed using isoform-specific SMARTpool siRNAs against ANKRD1, SERPINE1 and IL7R with Lipofectamine 3000 (Invitrogen) as the transfection reagent, according to the manufacturer's instructions. siRNAs were purchased from Dharmacon, Horizon Discovery, and a non-targeting siRNA was used as a negative control (Supplementary Table 7).

Bromodeoxyuridine cell proliferation assay

Measurements of cell proliferation in HCFs and HCMECs were conducted using a Cell Proliferation ELISA, bromodeoxyuridine (BrdU) (colorimetric) kit (Roche), following the manufacturer's protocol. HCF cells and HCMECs were seeded in 48-well plates at 48 h after siRNA transfection; cells were then serum starved for 24 h, followed by a 2-h incubation with BrdU labeling solution. Cells were washed with PBS and fixed with FixDenat solution, followed by incubation with tetramethylbenzidine (TMB) solution until color development. Absorbance was measured at a wavelength of 370 nm with reference at 492 nm using a TECAN Infinite M200 PRO microplate reader.

Wound healing assay

The HCFs were transiently transfected with siRNA for 48 h, then a cell suspension (5×10^5 cells ml^{-1}) from siRNA-transfected cells was added to each well of the Culture-Inserts 2 Well (Ibidi). The cells were incubated at 37 °C and 5% CO_2 for 24 h. The images were captured at 1 h and 24 h post-insert removal using a ×4 objective lens on a Leica DM 6000B microscope. The wound area was oriented vertically during image acquisition. The microscopic pictures were analyzed using ImageJ software with the wound healing plugin.

Endothelial cell tubulogenesis assay

HCMECs were transfected with siRNA for 48 h. Before cell seeding, the Matrigel Basement Membrane Matrix Growth Factor Reduced (Corning) was applied to each well. The cell suspension (2×10^5 cells ml^{-1}) from siRNA-transfected cells was added to each well of μ-slide. Images were collected at different time points (1 h and 24 h) using a ×4 objective lens on a Leica DM 6000B microscope. The microscopic pictures were analyzed using ImageJ software with the angiogenesis analyzer plugin.

RNA isolation from the cardiac cells and rat RV tissue, and RT-qPCR

Total RNA was extracted from cardiac cells (HCFs and HCMECs) and right ventricles of rat animal models (PAB and MCT) using the RNeasy Mini Kit (Qiagen) following the manufacturer's instructions. The cDNA synthesis was performed on equal amounts of RNA using the High-Capacity cDNA Reverse Transcription Kit with RNase Inhibitor (Thermo Fisher Scientific) according to the manufacturer's instructions. RT-qPCR was performed using iTaq Universal SYBR Green Supermix (BioRad) in the CFX96 Real-Time PCR detection system (BioRad). Gene expression was determined using the ΔCt method as previously described[65]. Hypoxanthine phosphoribosyltransferase 1 (HPRT1) and glyceraldehyde 3-phosphate dehydrogenase (GAPDH) were used as a reference gene (endogenous control). Intron-spanning human and rat-specific primers were designed using sequence information from the NCBI database and were purchased from Metabion International AG, Sigma-Aldrich and Merck KGaA, respectively (Supplementary Tables 8 and 9).

Reporting summary

Further information on research design is available in the Nature Portfolio Reporting Summary linked to this article.

Data availability

The RNA-seq data of human CTEPH cohorts and the control participants have been submitted to the Gene Expression Omnibus under accession number GSE249697. All data related to the findings of this study are available in the Article and Supplementary Information. Source data are provided with this paper.

Code availability

The code for this study is available via GitHub at https://github.com/loosolab/Code_Jafari_et_al_2024_cteph_rv_reverse_remodeling.

References

1. Benza, R. L. et al. Predicting survival in pulmonary arterial hypertension: insights from the Registry to Evaluate Early and Long-Term Pulmonary Arterial Hypertension Disease Management (REVEAL). *Circulation* **122**, 164–172 (2010).
2. Voelkel, N. F. et al. Right ventricular function and failure: report of a National Heart, Lung, and Blood Institute working group on cellular and molecular mechanisms of right heart failure. *Circulation* **114**, 1883–1891 (2006).
3. Iino, M., Dymarkowski, S., Chaothawee, L., Delcroix, M. & Bogaert, J. Time course of reversed cardiac remodeling after pulmonary endarterectomy in patients with chronic pulmonary thromboembolism. *Eur. Radiol.* **18**, 792–799 (2008).
4. Berman, M. et al. Right ventricular reverse remodeling after pulmonary endarterectomy: magnetic resonance imaging and clinical and right heart catheterization assessment. *Pulm. Circ.* **4**, 36–44 (2014).
5. di Salvo, T. G. et al. Right ventricular myocardial biomarkers in human heart failure. *J. Card. Fail.* **21**, 398–411 (2015).
6. Boucherat, O. et al. Identification of LTBP-2 as a plasma biomarker for right ventricular dysfunction in human pulmonary arterial hypertension. *Nat. Cardiovasc. Res.* **1**, 748–760 (2022).
7. Khassafi, F. et al. Transcriptional profiling unveils molecular subgroups of adaptive and maladaptive right ventricular remodeling in pulmonary hypertension. *Nat. Cardiovasc. Res.* **2**, 917–936 (2023).
8. Humbert, M. et al. 2022 ESC/ERS Guidelines for the diagnosis and treatment of pulmonary hypertension: developed by the task force for the diagnosis and treatment of pulmonary hypertension of the European Society of Cardiology (ESC) and the European Respiratory Society (ERS). Endorsed by the International Society for Heart and Lung Transplantation (ISHLT) and the European Reference Network on rare respiratory diseases (ERN-LUNG). *Eur. Heart J.* **43**, 3618–3731 (2022).
9. McCabe, C. et al. Right ventricular dysfunction in chronic thromboembolic obstruction of the pulmonary artery: a pressure–volume study using the conductance catheter. *J. Appl. Physiol.* **116**, 355–363 (2014).
10. Hardziyenka, M. et al. Right ventricular failure following chronic pressure overload is associated with reduction in left ventricular mass: evidence for atrophic remodeling. *J. Am. Coll. Cardiol.* **57**, 921–928 (2011).
11. Mayer, E. et al. Surgical management and outcome of patients with chronic thromboembolic pulmonary hypertension: results from an international prospective registry. *J. Thorac. Cardiovasc. Surg.* **141**, 702–710 (2011).
12. Maschke, S. K. et al. MRI-derived regional biventricular function in patients with chronic thromboembolic pulmonary hypertension before and after pulmonary endarterectomy. *Acad. Radiol.* **25**, 1540–1547 (2018).
13. Surie, S. et al. Effect of pulmonary endarterectomy for chronic thromboembolic pulmonary hypertension on stroke volume response to exercise. *Am. J. Cardiol.* **114**, 136–140 (2014).
14. Reesink, H. J. et al. Reverse right ventricular remodeling after pulmonary endarterectomy in patients with chronic thromboembolic pulmonary hypertension: utility of magnetic resonance imaging to demonstrate restoration of the right ventricle. *J. Thorac. Cardiovasc. Surg.* **133**, 58–64 (2007).
15. Maybaum, S. et al. Cardiac improvement during mechanical circulatory support: a prospective multicenter study of the LVAD Working Group. *Circulation* **115**, 2497–2505 (2007).
16. Barbone, A. et al. Comparison of right and left ventricular responses to left ventricular assist device support in patients with severe heart failure: a primary role of mechanical unloading underlying reverse remodeling. *Circulation* **104**, 670–675 (2001).
17. Kim, G. H., Uriel, N. & Burkhoff, D. Reverse remodelling and myocardial recovery in heart failure. *Nat. Rev. Cardiol.* **15**, 83–96 (2018).
18. Frederiksen, C. A. et al. Reverse remodeling of tricuspid valve morphology and function in chronic thromboembolic pulmonary hypertension patients following pulmonary thrombo-endarterectomy: a cardiac magnetic resonance imaging and invasive hemodynamic study. *BMC Cardiovasc. Disord.* **21**, 450 (2021).
19. D'Armini, A. M. et al. Reverse right ventricular remodeling after pulmonary endarterectomy. *J. Thorac. Cardiovasc. Surg.* **133**, 162–168 (2007).
20. Sweet, M. E. et al. Transcriptome analysis of human heart failure reveals dysregulated cell adhesion in dilated cardiomyopathy and activated immune pathways in ischemic heart failure. *BMC Genomics* **19**, 812 (2018).
21. Ritchie, M. E. et al. limma powers differential expression analyses for RNA-sequencing and microarray studies. *Nucleic Acids Res.* **43**, e47 (2015).
22. Ramirez Flores, R. O. et al. Consensus transcriptional landscape of human end-stage heart failure. *J. Am. Heart Assoc.* **10**, e019667 (2021).
23. Boehm, M. et al. Delineating the molecular and histological events that govern right ventricular recovery using a novel mouse model of pulmonary artery de-banding. *Cardiovasc. Res.* **116**, 1700–1709 (2020).
24. Litviňuková, M. et al. Cells of the adult human heart. *Nature* **588**, 466–472 (2020).
25. Kanemaru, K. et al. Spatially resolved multiomics of human cardiac niches. *Nature* **619**, 801–810 (2023).
26. Uhlén, M. et al. Proteomics. Tissue-based map of the human proteome. *Science* **347**, 1260419 (2015).
27. Lüönd, F. et al. Hierarchy of TGFβ/SMAD, Hippo/YAP/TAZ, and Wnt/β-catenin signaling in melanoma phenotype switching. *Life Sci. Alliance* **5**, e202101010 (2022).
28. Delcroix, M. et al. Long-term outcome of patients with chronic thromboembolic pulmonary hypertension: results from an International Prospective Registry. *Circulation* **133**, 859–871 (2016).
29. Andersen, S., Nielsen-Kudsk, J. E., Vonk Noordegraaf, A. & de Man, F. S. Right ventricular fibrosis. *Circulation* **139**, 269–285 (2019).
30. Al-Qazazi, R. et al. Macrophage-NLRP3 activation promotes right ventricle failure in pulmonary arterial hypertension. *Am. J. Respir. Crit. Care Med.* **206**, 608–624 (2022).
31. Alabed, S. et al. Myocardial T1-mapping and extracellular volume in pulmonary arterial hypertension: a systematic review and meta-analysis. *Magn. Reson. Imaging* **79**, 66–75 (2021).
32. Chen, Y. et al. Impact of epicardial adipose tissue on right cardiac function and prognosis in pulmonary arterial hypertension. *Chest* **165**, 1211–1223 (2024).
33. Brittain, E. L. et al. Fatty acid metabolic defects and right ventricular lipotoxicity in human pulmonary arterial hypertension. *Circulation* **133**, 1936–1944 (2016).
34. Iacobellis, G. Epicardial adipose tissue in contemporary cardiology. *Nat. Rev. Cardiol.* **19**, 593–606 (2022).
35. Koepp, K. E., Obokata, M., Reddy, Y. N. V., Olson, T. P. & Borlaug, B. A. Hemodynamic and functional impact of epicardial adipose tissue in heart failure with preserved ejection fraction. *JACC Heart Fail.* **8**, 657–666 (2020).
36. Sun, X. Q., Abbate, A. & Bogaard, H. J. Role of cardiac inflammation in right ventricular failure. *Cardiovasc. Res.* **113**, 1441–1452 (2017).

37. Saito, T. et al. Effects of pulmonary endarterectomy on pulmonary hemodynamics in chronic thromboembolic pulmonary hypertension, evaluated by interventricular septum curvature. *Pulm. Circ.* **10**, 2045894019897502 (2020).
38. Sugiura, T. et al. Role of 320-slice CT imaging in the diagnostic workup of patients with chronic thromboembolic pulmonary hypertension. *Chest* **143**, 1070–1077 (2013).
39. Franco, D. et al. Left and right ventricular contributions to the formation of the interventricular septum in the mouse heart. *Dev. Biol.* **294**, 366–375 (2006).
40. Lankeit, M. et al. Pulmonary endarterectomy in chronic thromboembolic pulmonary hypertension. *J. Heart Lung Transplant.* **37**, P250–P258 (2017).
41. Lang, I. M., Dorfmüller, P. & Vonk Noordegraaf, A. The pathobiology of chronic thromboembolic pulmonary hypertension. *Ann. Am. Thorac. Soc.* **13**, S215–S221 (2016).
42. Kriechbaum, S. D. et al. N-terminal pro-B-type natriuretic peptide for monitoring after balloon pulmonary angioplasty for chronic thromboembolic pulmonary hypertension. *J. Heart Lung Transplant.* **37**, 639–646 (2018).
43. Kriechbaum, S. D. et al. Cardiac biomarkers as indicators of right ventricular dysfunction and recovery in chronic thromboembolic pulmonary hypertension patients after balloon pulmonary angioplasty therapy—a cardiac magnetic resonance imaging cohort study. *Pulm. Circ.* **11**, 20458940211056500 (2021).
44. Kriechbaum, S. D. et al. Mid-regional pro-atrial natriuretic peptide and copeptin as indicators of disease severity and therapy response in CTEPH. *ERJ Open Res.* **6**, 00356–02020 (2020).
45. Wiedenroth, C. B. et al. Riociguat and balloon pulmonary angioplasty improve prognosis in patients with inoperable chronic thromboembolic pulmonary hypertension. *J. Heart Lung Transplant.* **42**, 134–139 (2023).
46. Roller, F. C. et al. Correlation of native T1 mapping with right ventricular function and pulmonary haemodynamics in patients with chronic thromboembolic pulmonary hypertension before and after balloon pulmonary angioplasty. *Eur. Radiol.* **29**, 1565–1573 (2019).
47. Roller, F. C. et al. Effects of BPA on right ventricular mechanical dysfunction in patients with inoperable CTEPH—a cardiac magnetic resonance study. *Eur. J. Radiol.* **147**, 110111 (2022).
48. Bogomolovas, J. et al. Induction of Ankrd1 in dilated cardiomyopathy correlates with the heart failure progression. *Biomed. Res. Int.* **2015**, 273936 (2015).
49. Ling, S. S. M., Chen, Y.-T., Wang, J., Richards, A. M. & Liew, O. W. Ankyrin repeat domain 1 protein: a functionally pleiotropic protein with cardiac biomarker potential. *Int. J. Mol. Sci.* **18**, 1362 (2017).
50. Murphy, N. P., Lubbers, E. R. & Mohler, P. J. Advancing our understanding of AnkRD1 in cardiac development and disease. *Cardiovasc. Res.* **116**, 1402–1404 (2020).
51. Ghosh, A. K. & Vaughan, D. E. PAI-1 in tissue fibrosis. *J. Cell. Physiol.* **227**, 493–507 (2012).
52. Galiè, N. et al. 2015 ESC/ERS Guidelines for the diagnosis and treatment of pulmonary hypertension: The Joint Task Force for the Diagnosis and Treatment of Pulmonary Hypertension of the European Society of Cardiology (ESC) and the European Respiratory Society (ERS): endorsed by: Association for European Paediatric and Congenital Cardiology (AEPC), International Society for Heart and Lung Transplantation (ISHLT). *Eur. Heart J.* **37**, 67–119 (2016).
53. Andrews, S. FastQC: a quality control tool for high throughput sequence data. https://www.bioinformatics.babraham.ac.uk/projects/fastqc/ (2010).
54. Bolger, A. M., Lohse, M. & Usadel, B. Trimmomatic: a flexible trimmer for Illumina sequence data. *Bioinformatics* **30**, 2114–2120 (2014).
55. Dobin, A. et al. STAR: ultrafast universal RNA-seq aligner. *Bioinformatics* **29**, 15–21 (2013).
56. Liao, Y., Smyth, G. K. & Shi, W. featureCounts: an efficient general purpose program for assigning sequence reads to genomic features. *Bioinformatics* **30**, 923–930 (2014).
57. Love, M. I., Huber, W. & Anders, S. Moderated estimation of fold change and dispersion for RNA-seq data with DESeq2. *Genome Biol.* **15**, 550 (2014).
58. Lê, S., Josse, J. & Husson, F. FactoMineR: an R package for multivariate analysis. *J. Stat. Softw.* **25**, 1–18 (2008).
59. Leek, J. T., Johnson, W. E., Parker, H. S., Jaffe, A. E. & Storey, J. D. The sva package for removing batch effects and other unwanted variation in high-throughput experiments. *Bioinformatics* **28**, 882–883 (2012).
60. Gu, Z., Eils, R. & Schlesner, M. Complex heatmaps reveal patterns and correlations in multidimensional genomic data. *Bioinformatics* **32**, 2847–2849 (2016).
61. Gu, Z. Complex heatmap visualization. *Imeta* **1**, e43 (2022).
62. Zhou, Y. et al. Metascape provides a biologist-oriented resource for the analysis of systems-level datasets. *Nat. Commun.* **10**, 1523 (2019).
63. R Core Team R: A Language and Environment for Statistical Computing (R Foundation for Statistical Computing, 2024); http://www.R-project.org/
64. Kojonazarov, B. et al. Single- versus multiple-beat measurement of right ventricular function in rodents. *Am. J. Respir. Cell Mol. Biol.* **71**, 133–135 (2024).
65. Pullamsetti, S. S. et al. Lung cancer-associated pulmonary hypertension: role of microenvironmental inflammation based on tumor cell-immune cell cross-talk. *Sci. Transl. Med.* **9**, eaai9048 (2017).

Acknowledgements

This study was funded by the German Research Foundation (DFG), Collaborative Research Center (CRC) 1213 (projects A01 and A05 grants to S.S.P.; project CP01 grants to C.L., E.M., P.D. and C.B.W.; project CP02 granted to B.K.; project B04 granted to R.T.S.; project B07 granted to O.D., H.N. and C.W.H.; projects A08 and B08 granted to H.A.G.; projects A06 and A07 granted to N.W.; and European Research Council (ERC) Consolidator Grant (866051 to S.S.P.). W.S., S.S.P., R.T.S., P.D. and N.W., are supported by the Excellence Cluster Cardio Pulmonary Institute (CPI; EXC2026) and the German Center for Lung Research (DZL), and W.S. and S.S.P. are supported by the Max Planck Society. L.J., D.G. and P.C. are funded by the DFG CRC 1213. P.L., Z.V.V. and P.F. received funding from the HUN-REN Hungarian Research Network, from Momentum Research Grant from the Hungarian Academy of Sciences (LP- 2021-14), from the European Union's Horizon 2020 research and innovation program under grant agreement number 739593. Project number RRF-2.3.1-21-2022-00003 has been implemented with the support provided by the European Union. Project number 2022-1.1.1-KK-2022-00005 has been implemented with the support provided by the Ministry of Innovation and Technology of Hungary from the National Research, Development and Innovation Fund. Project number TKP2021-EGA-23 has been implemented with support provided by the Ministry of Innovation and Technology of Hungary from the National Research, Development and Innovation Fund, financed under the TKP2021-EGA funding scheme. M.B. received funding from the Max Kade Foundation, and E.S. received grants from NIH/National Heart and Lung Blood Institute - R01HL158868 and US Department of Defense W81XWH-17-1-0327. We would like to acknowledge the technical contributions of M. Rieschel and N. Staubach (Justus Liebig University, Medical Clinic I, Cardiology and Angiology, Giessen, Germany), S. Sass (Department of Experimental Cardiology, Kerckhoff Clinic), E. Bieniek (Universities of Giessen and Marburg Lung Center), and U. Eule, N. Wilker,

J. Rostkovius and D. Grella (Max Planck Institute for Heart and Lung Research, Bad Nauheim, Germany).

Author contributions

L.J., C.B.W., C.L., W.S., E.M, S. Guth and S.S.P. conceived and designed the research study. L.J., S.D.K., D.G., P.C., S. Guenther, C.K., A.M.S., A.V.C., C.T., J.W., S.K., T.K., R.T.S., O.D., H.N., C.W.H., H.A.G., P.D. and N.W. conducted the experiments, and analyzed and organized the preclinical and clinical data. C.B.W., S. Guth, P.L., Z.V.V., P.F., E.M. and C.L. provided the samples. B.K. provided rat animal models and hemodynamic and echo data. M.B. and E.S. provided the mice array data. L.J., W.S., C.B.W., C.L. and S.S.P. drafted the paper. All authors offered critical feedback and contributed to the research, analysis and paper development.

Funding

Open access funding provided by Justus-Liebig-Universität Gießen.

Competing interests

The authors declare no competing interests.

Additional information

Extended data is available for this paper at https://doi.org/10.1038/s44161-025-00672-8.

Supplementary information The online version contains supplementary material available at https://doi.org/10.1038/s44161-025-00672-8.

Correspondence and requests for materials should be addressed to Christoph Liebetrau or Soni Savai Pullamsetti.

Peer review information *Nature Cardiovascular Research* thanks Kory Lavine and the other, anonymous, reviewer(s) for their contributon to the peer review of this work.

Leili Jafari[1,2,17], Christoph B. Wiedenroth[3,17], Steffen D. Kriechbaum[4,5], Dimitri Grün[4,5], Prakash Chelladurai[1,6], Stefan Guenther[1], Carsten Kuenne[1], Alicia M. Späth[6,7], Anoop V. Cherian[1,6], Christian Troidl[4,5], Jochen Wilhelm[6,7], Stanislav Keranov[2], Till Keller[4,5], Baktybek Kojonazarov[6,7], Ralph T. Schermuly[6,7], Stefan Guth[3], Oliver Dörr[2], Holger Nef[2], Mario Boehm[8,9], Edda Spiekerkoetter[8,9], Przemyslaw Leszek[10], Zoltan V. Varga[11,12,13], Peter Ferdinandy[11,14,15,16], Hossein A. Ghofrani[6], Peter Dorfmüller[6,7], Norbert Weißmann[6], Christian W. Hamm[2,4,5], Eckhard Mayer[3], Werner Seeger[1,6,7], Christoph Liebetrau[4,5,17] ✉ & Soni Savai Pullamsetti[1,6,7,17] ✉

[1]Max-Planck Institute for Heart and Lung Research, Bad Nauheim, Germany. [2]Department of Internal Medicine I, Justus Liebig University, Giessen, Germany. [3]Department of Thoracic Surgery, Kerckhoff Heart and Lung Center, Bad Nauheim, Germany. [4]Department of Cardiology, Kerckhoff Heart and Lung Center, Bad Nauheim, Germany. [5]Partner Site Rhein-Main, DZHK (German Center for Cardiovascular Research), Frankfurt am Main, Germany. [6]Department of Internal Medicine II/V, Universities of Giessen and Marburg Lung Center (UGMLC), Member of the German Center for Lung Research (DZL), Excellence Cluster Cardio-Pulmonary Institute (CPI), Justus-Liebig University, Giessen, Germany. [7]Institute for Lung Health, Justus Liebig University, Giessen, Germany. [8]Vera Moulton Wall Center for Pulmonary Vascular Disease, Stanford School of Medicine, Stanford University, Stanford, CA, USA. [9]Cardiovascular Institute, Stanford University, Stanford, CA, USA. [10]Heart Failure and Transplantology Department, Mechanical Circulatory Support and Transplant Department, National Institute of Cardiology, Warsaw, Poland. [11]Department of Pharmacology and Pharmacotherapy, Semmelweis University, Budapest, Hungary. [12]HCEMM-SU Cardiometabolic Immunology Research Group, Department of Pharmacology and Pharmacotherapy, Semmelweis University, Budapest, Hungary. [13]Momentum-SU Cardio-oncology and Cardioimmunology Research Group, Budapest, Hungary. [14]Center for Pharmacology and Drug Research & Development, Semmelweis University, Budapest, Hungary. [15]HUN-REN-SU System Pharmacology Research Group, Department of Pharmacology and Pharmacotherapy, Semmelweis University, Budapest, Hungary. [16]Pharmahungary Group, Szeged, Hungary. [17]These authors contributed equally: Leili Jafari, Christoph B. Wiedenroth, Christoph Liebetrau, Soni Savai Pullamsetti. ✉e-mail: c.liebetrau@ccb.de; Soni.Pullamsetti@innere.med.uni-giessen.de

https://doi.org/10.1038/s44161-025-00672-8

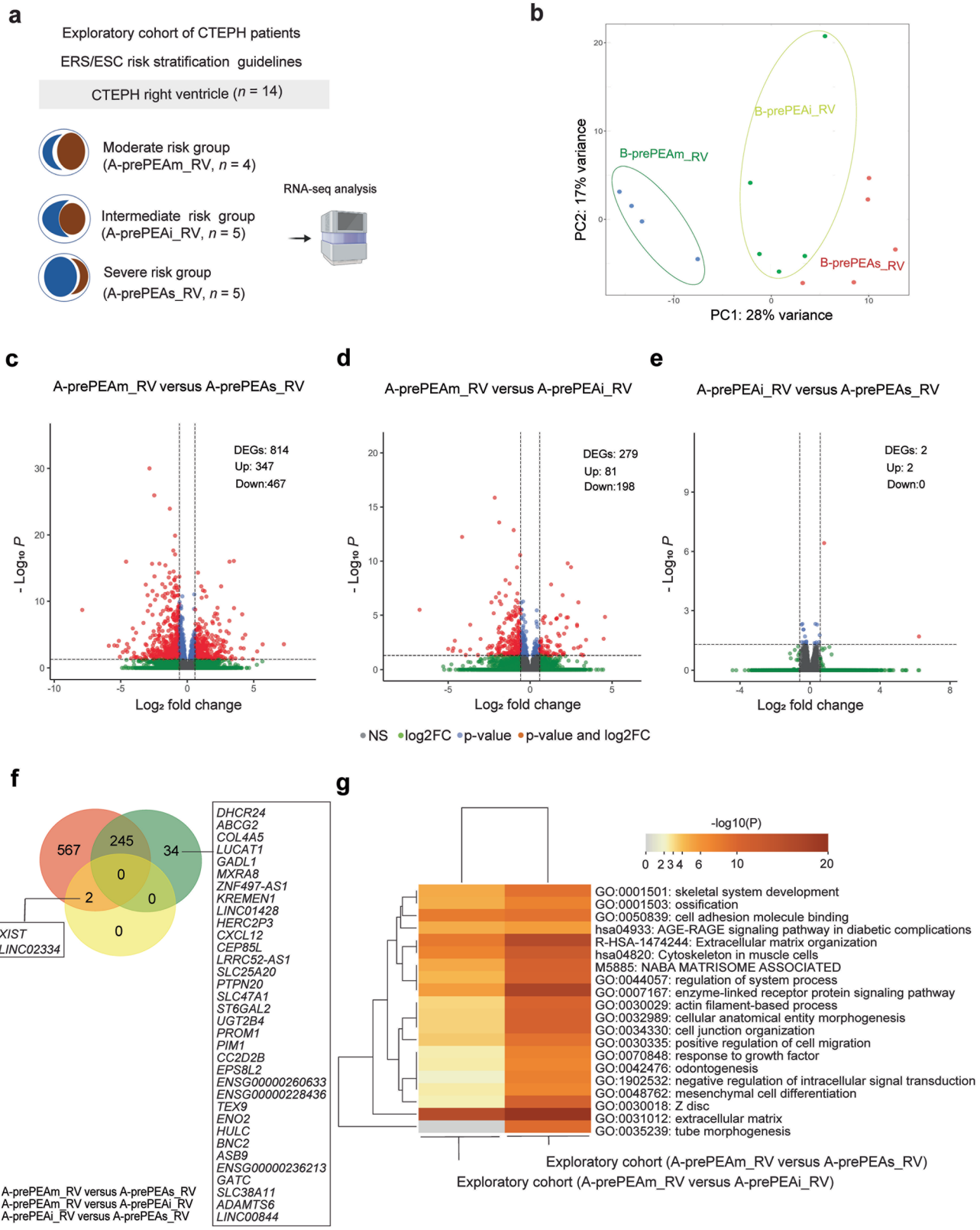

Extended Data Fig. 1 | See next page for caption.

https://doi.org/10.1038/s44161-025-00672-8

Extended Data Fig. 1 | Transcriptomic profiling of the right ventricle in the exploratory cohort of patients with CTEPH. a, In the exploratory cohort, RNA-seq analysis was performed on the RV of patients with CTEPH before PEA (A-prePEA_RV, $n = 14$), and patients were classified into three risk groups, including A-prePEAm_RV ($n = 4$), A-prePEAi_RV ($n = 5$), and A-prePEAs_RV ($n = 5$). Illustration created using Biorender.com. **b**, Principal component analysis (PCA) plot depicting the RV transcriptomic profile from 14 samples. The colors represent the distinct status of the RV. Volcano plot showing the distribution of each gene in **c**, A-prePEAm_RV versus A-prePEAs_RV, **d**, A-prePEAm_RV versus A-prePEAi_RV, and **e**, A-prePEAi_RV versus A-prePEAs_RV, of the exploratory cohort of patients with CTEPH. The significant differentially expressed genes (DEGs) ($|\log2FC| \geq 0.585$ and $P_{adj} \leq 0.05$, two-sided) were discriminated based on the P value < 0.05 and $|\log2FC| > 0.585$ (in red), only P value (blue), log2FC (green), and not significant in grey dots. **f**, Venn diagrams of DEGs display the common and distinct DEGs among the three groups of A-prePEAm_RV versus A-prePEAs_RV, A-prePEAm_RV versus A-prePEAi_RV, and A-prePEAi_RV versus A-prePEAs_RV in the exploratory cohort of patients with CTEPH. **g**, Heatmap shows the top 20 overrepresented clusters of terms for all the DEGs between the following comparisons: A-prePEAm_RV versus A-prePEAi_RV and A-prePEAm_RV versus A-prePEAs_RV.

https://doi.org/10.1038/s44161-025-00672-8

Extended Data Fig. 2 | Pathway enrichment analysis in the RV of the exploratory and confirmatory cohorts of patients with CTEPH before PEA. The clustered heatmap shows top 100 overrepresented GO terms and pathways for both cohorts in following comparisons: B-prePEAm_RV versus B-prePEAs_RV, A-prePEAm_RV versus A-prePEAs_RV, B-prePEAi_RV versus B-prePEAs_RV, and B-prePEAm_RV versus B-prePEAi_RV.

https://doi.org/10.1038/s44161-025-00672-8

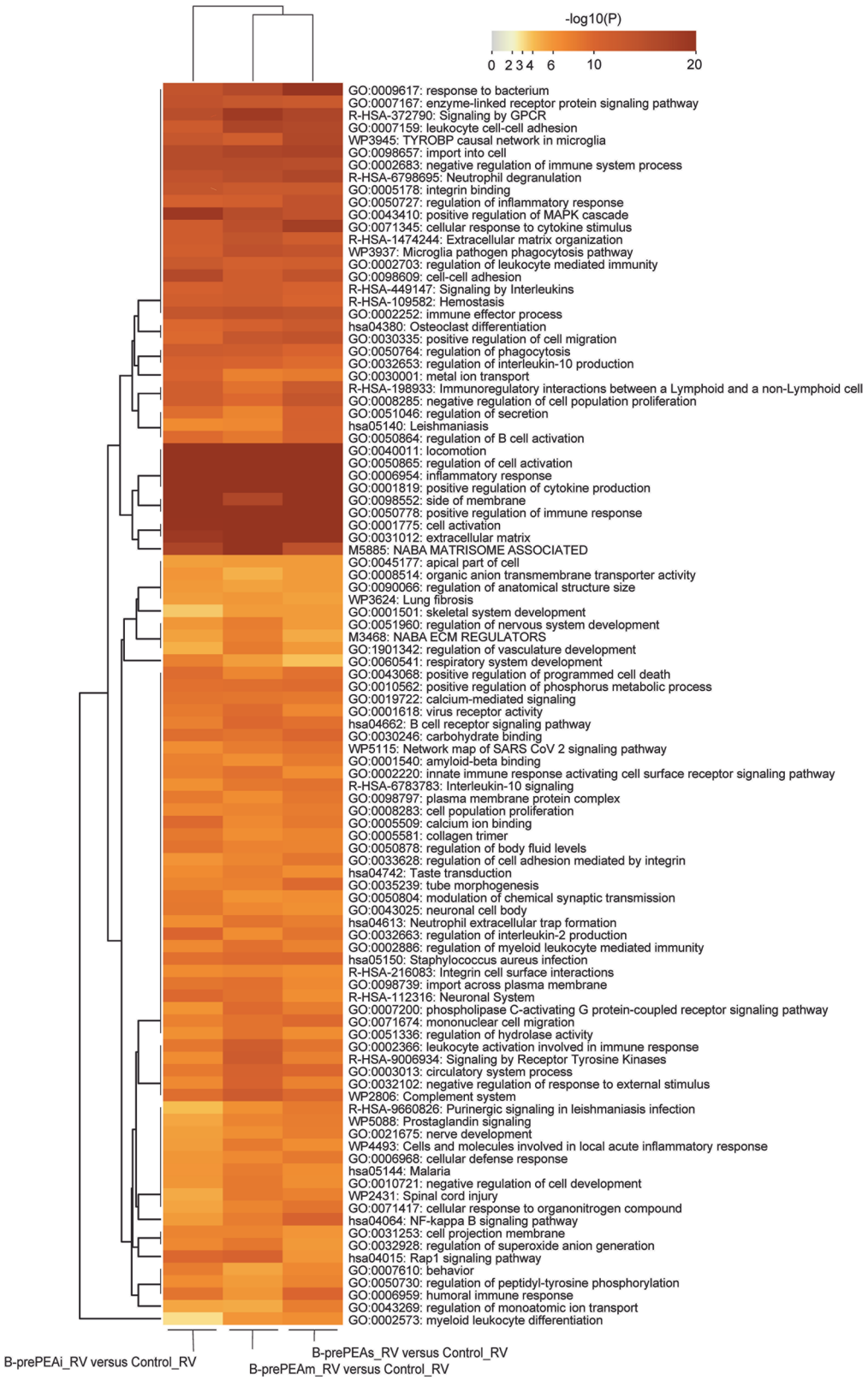

Extended Data Fig. 3 | Pathway enrichment analysis in the CTEPH RV of the confirmatory cohort versus control RV. The clustered heatmap displays the top 100 overrepresented GO terms and pathways resulting from the comparisons between B-prePEAi_RV versus Control_RV, B-prePEAm_RV versus Control_RV, and B-prePEAs_RV versus Control_RV.

https://doi.org/10.1038/s44161-025-00672-8

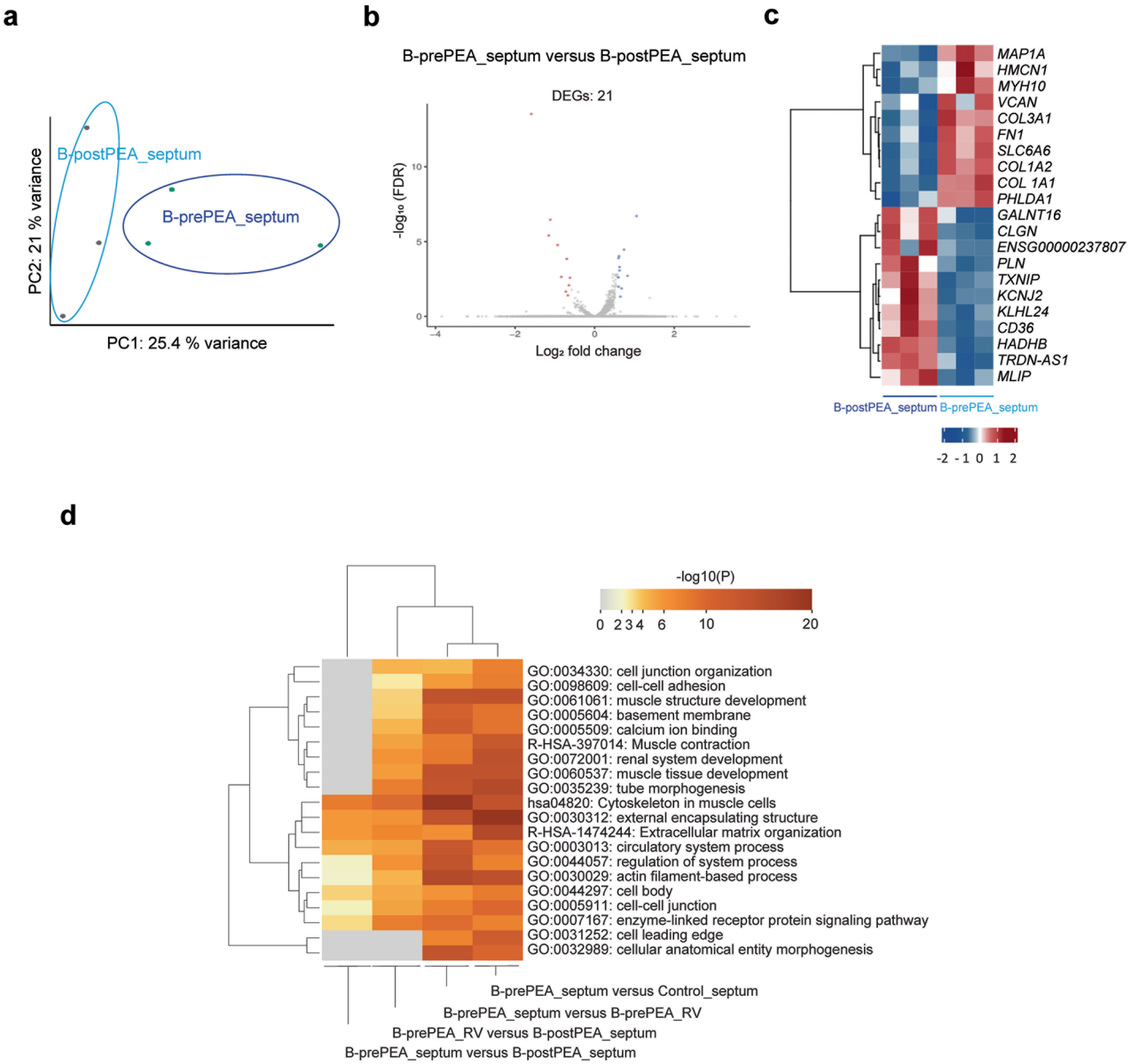

Extended Data Fig. 4 | Analysis of the transcriptomic profile of the septum before and after PEA in the confirmatory cohort of patients with CETPH. **a**, PCA plot illustrates the septum before PEA (B-prePEA_septum, $n = 3$) and after PEA (B-postPEA_septum, $n = 3$). **b**, Volcano plot displays the significant DEGs (base mean ≥5; |log2FC | ≥ 0.585; FDR ≤ 0.05) in B-prePEA_septum (red) versus B-postPEA_septum (blue). **c**, Heatmap shows the top significant DEGs in B-prePEA_septum versus B-postPEA_septum. The scaled z-score of normalized counts is shown. **d**, The heatmap illustrates the top 20 overrepresented clusters of terms associated with DEGs in the following comparisons: B-prePEA_septum versus B-postPEA_septum, B-prePEA_RV versus B-postPEA_septum, B-prePEA_septum versus B-prePEA_RV, and B-prePEA_septum versus Control_septum.

https://doi.org/10.1038/s44161-025-00672-8

Extended Data Fig. 5 | Pathway enrichment analysis in the CTEPH septum of the confirmatory cohort versus control septum. The clustered heatmap displays the top 100 overrepresented GO terms and pathways resulting from the comparisons between B-prePEA_septum versus B-prePEA_RV, B-prePEA_septum versus Control_septum, B-prePEA_RV versus B-postPEA_septum, B-prePEA_septum versus B-postPEA_septum.

https://doi.org/10.1038/s44161-025-00672-8

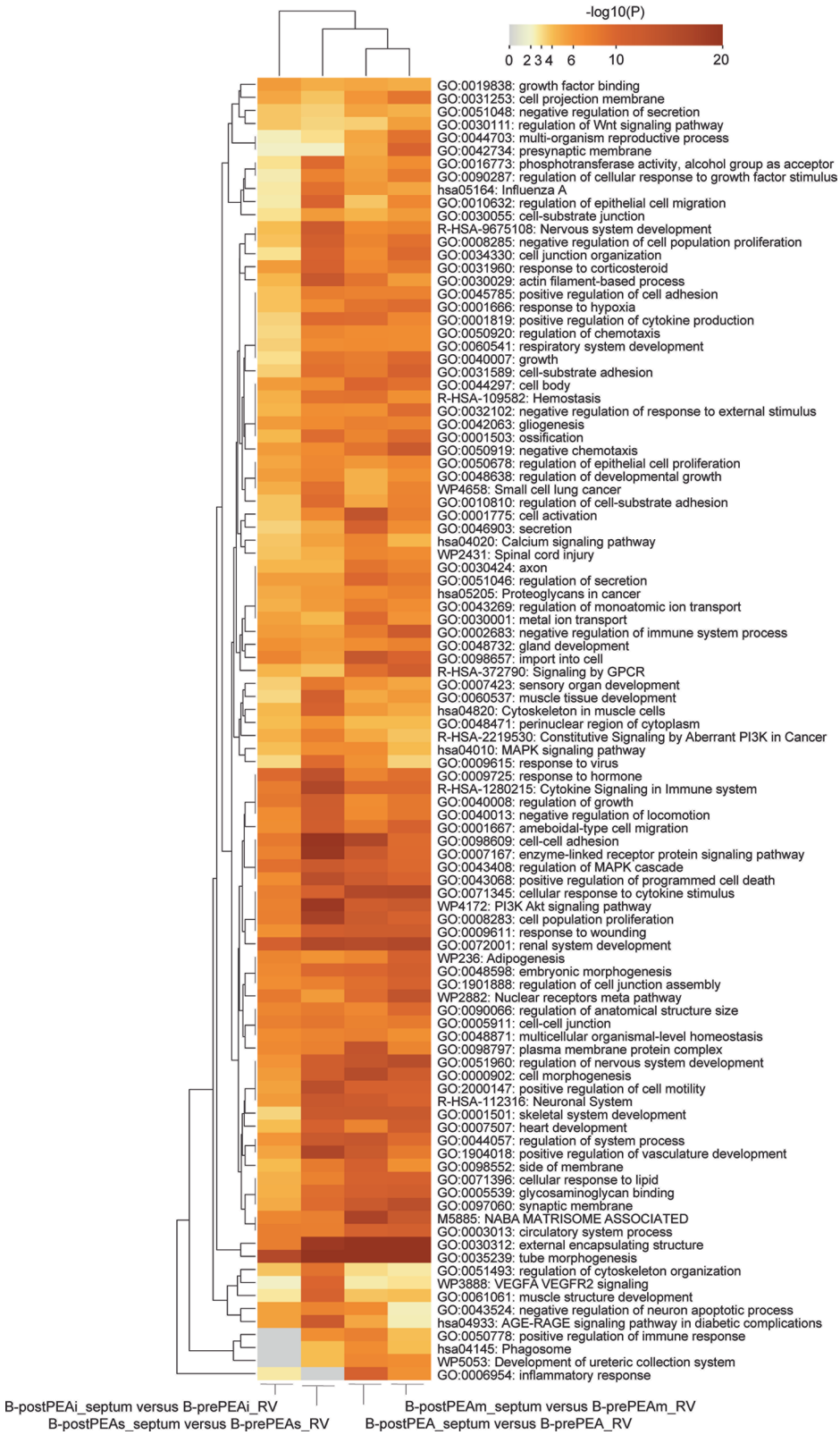

Extended Data Fig. 6 | Pathway enrichment analysis in the confirmatory cohort of CTEPH patients before and after PEA. The clustered heatmap shows the top 100 overrepresented GO terms and pathways resulting from four comparisons, including: B-postPEAi_septum versus B-prePEAi_RV, B-postPEAs_septum versus B-prePEAs_RV, B-postPEA_septum versus B-prePEA_RV, and B-postPEAm_septum versus B-prePEAm_RV.

https://doi.org/10.1038/s44161-025-00672-8

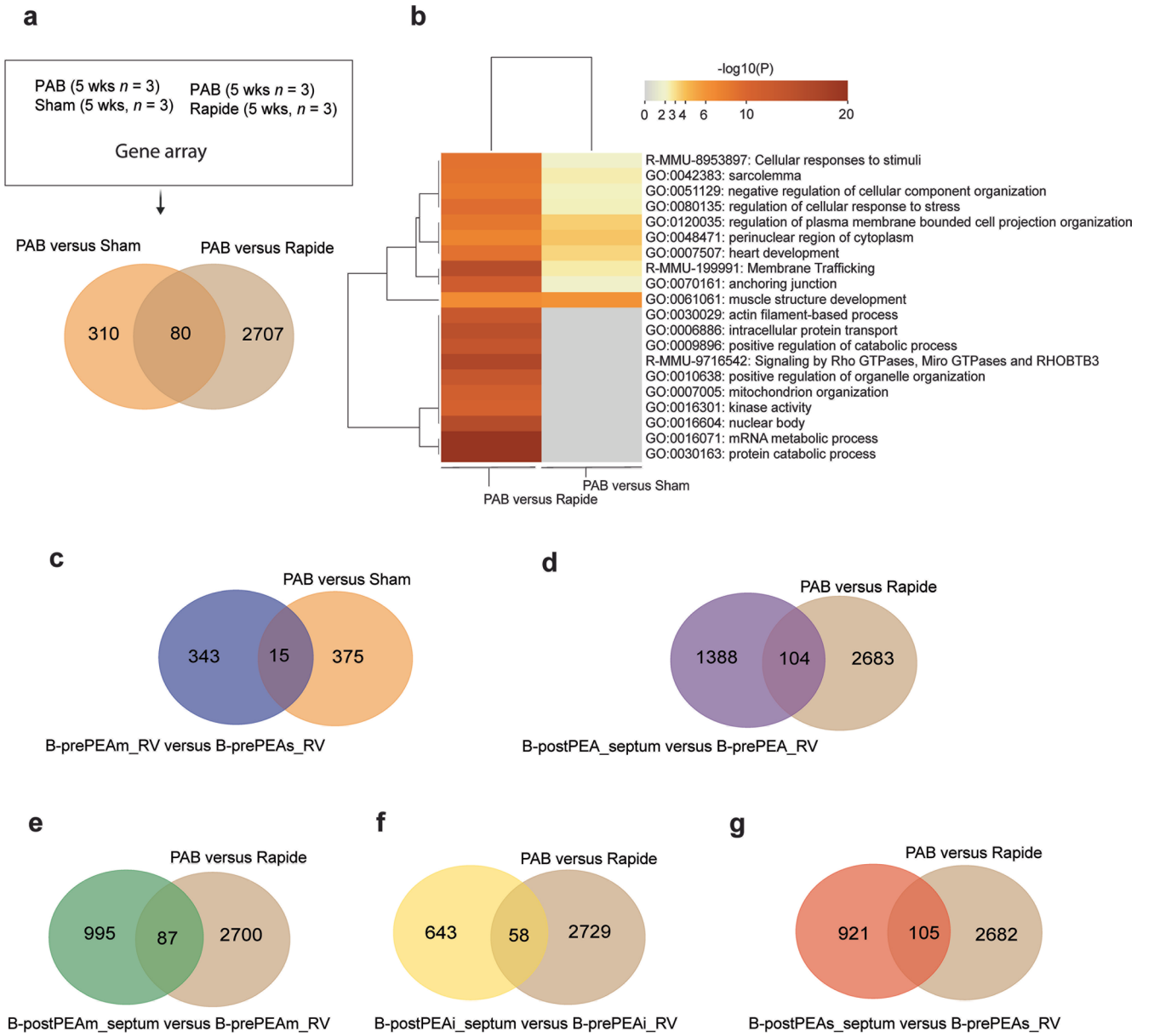

Extended Data Fig. 7 | Gene expression profile in the RV of the PAB banding and de-banding mouse model. a, Venn diagram shows the common and specific genes in PAB versus Sham and PAB versus Rapide. **b**, Heatmap visualizes the top 20 overrepresented clusters of terms for all differentially expressed genes among PAB versus Sham and PAB versus Rapide. **c-g**, Venn diagrams showing the common and specific genes among (**c**) B-prePEAm_RV versus B-prePEAs_RV and PAB versus Sham, (**d**) B-postPEA_septum versus B-prePEA_RV and PAB versus Rapide, (**e**) B-postPEAm_septum versus B-prePEAm_RV and PAB versus Rapide, (**f**) B-postPEAi_septum versus B-prePEAi_RV and PAB versus Rapide, and, (**g**) B-postPEAs_septum versus B-prePEAs_RV and PAB versus Rapide. The source data for the re-analyzed data is from ref. 23.

https://doi.org/10.1038/s44161-025-00672-8

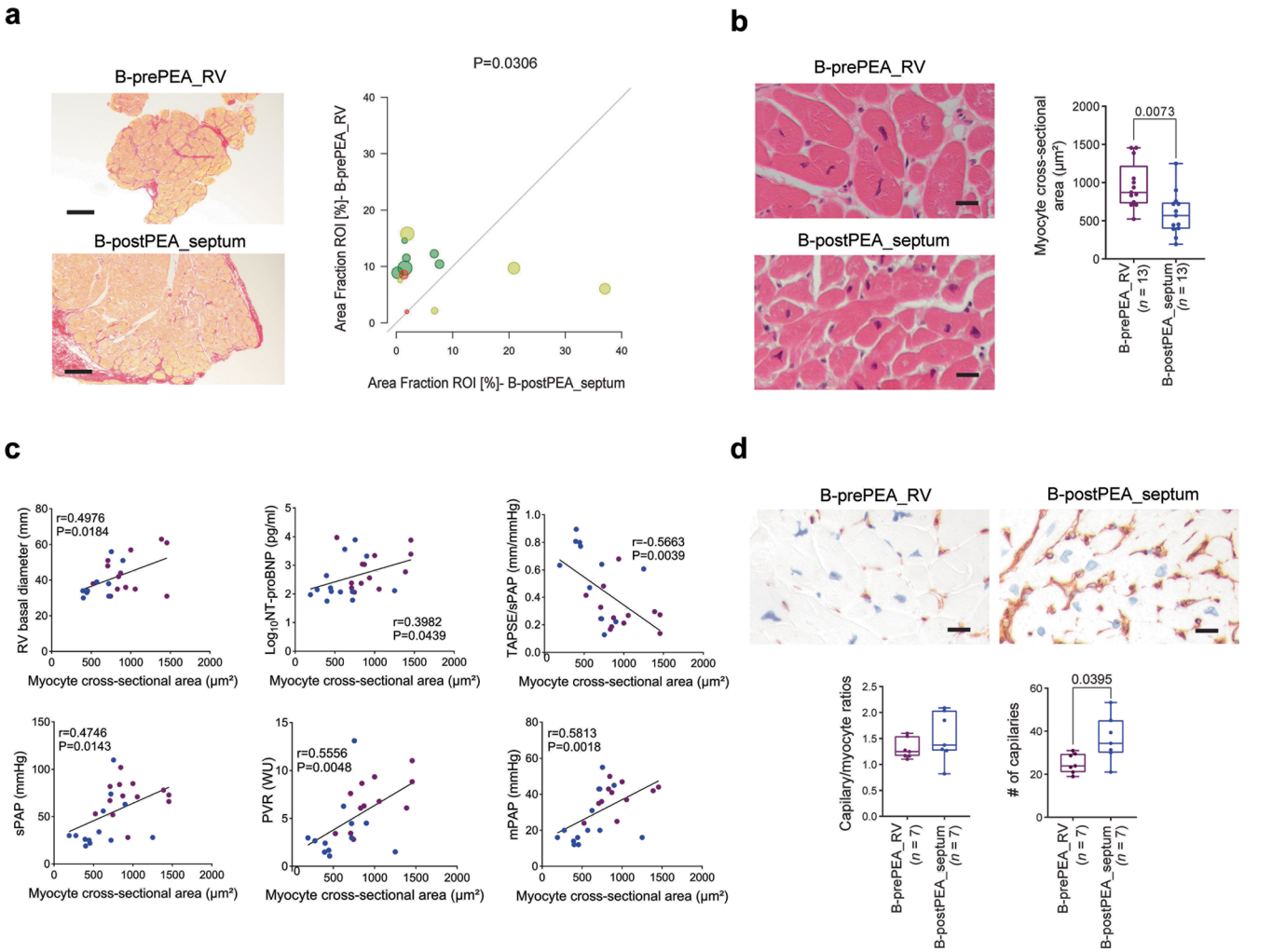

Extended Data Fig. 8 | Hypertrophy and fibrosis in the confirmatory cohort of patients with CTEPH at prePEA_RV and postPEA_septum. a, Representative images and corresponding quantification of Sirius red-stained tissue sections of RV (B-prePEA_RV, $n = 13$ patients with a total of 47 fibrosis tissue sections) and septum (B-postPEA_septum, $n = 13$ patients with a total of 13 fibrosis tissue sections) in paired patient samples of the confirmatory cohort of patients with CTEPH. The area fractions were compared using a paired-sample t-test on the log fractions, using the total tissue area per patient as weights. Scale bar, 100 µm. **b**, Representative images and corresponding quantification of the cross-sectional view of the myocytes on H&E staining of RV (B-prePEA_RV, $n = 13$) and septum (B-postPEA_septum, $n = 13$) in paired patient samples from the confirmatory cohort of patients with CTEPH are displayed. Data are presented as mean ± SEM and *P* value was calculated by two-tailed paired t-test. Scale bar, 20 µm. **c**, Pearson correlation coefficient (r), and its associated two-tailed *P* value was performed between myocyte cross-sectional area and various clinical parameters. **d**, In the confirmatory cohort of CTEPH patients, paired tissue samples from the RV (B-prePEA_RV, $n = 7$) and septum (B-postPEA_septum, $n = 7$) were examined. Representative images and quantification of capillary/myocyte ratios, as well as the number of capillaries, are presented for both regions. Data are presented as mean ± SEM and *P* value was calculated by two-tailed paired t-test. Scale bar: 20 µm. Boxes show the interquartile range (IQR, 25th to 75th percentile), and the central bands indicate the median. The whiskers extend to 1.5 times the IQR above and below the box.

https://doi.org/10.1038/s44161-025-00672-8

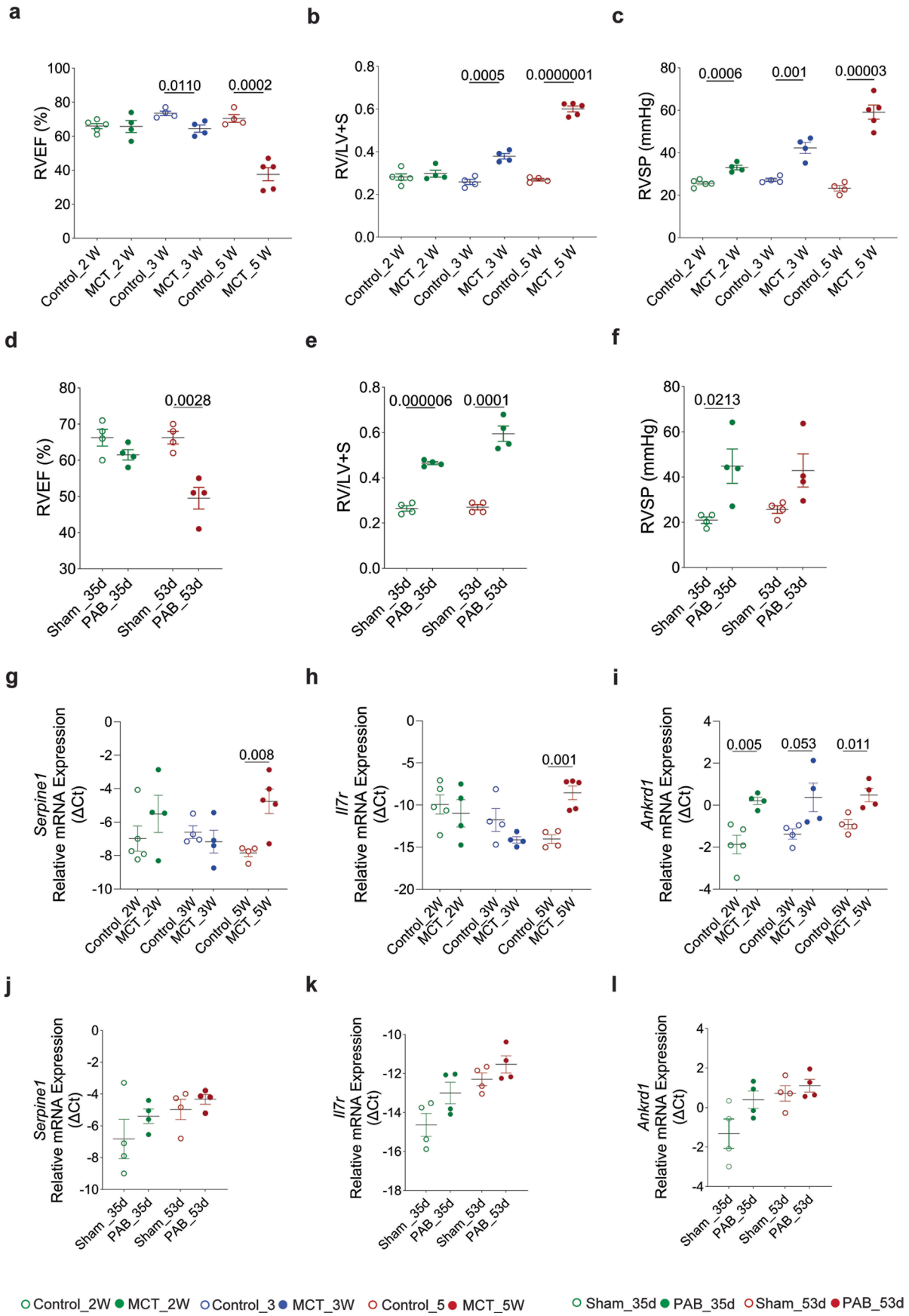

Extended Data Fig. 9 | See next page for caption.

https://doi.org/10.1038/s44161-025-00672-8

Extended Data Fig. 9 | Assessment of hemodynamics parameters and RV function in MCT-induced PH and PAB rat models and *Serpine1*, *Il7r*, and *Ankrd1* gene expression validation in corresponding RV tissues. a, RV ejection fraction (RVEF), **b**, RV hypertrophy (the ratio of RV to LV+ septum), and **c**, RV systolic pressure (RVSP) in MCT-induced PH rats are presented for 2 W (weeks) (Control_2W, *n* = 5, and MCT _2W, *n* = 4), for 3 W rats (Control_3W, *n* = 4 and MCT _3W, *n* = 4), and 5 W rats (Control_5W, *n* = 4 and MCT_5W, *n* = 5). **d**, RVEF, **e**, RV/LV + S, and **f**, RVSP in PAB rat models are shown for two time points: 35 d (days) (Sham_35d, *n* = 4 and PAB_35d, *n* = 4), and for 53 d (Sham_53d, *n* = 4 and PAB _53d, *n* = 4). The relative mRNA expression levels of *Serpine1* (**g**), *Il7r* (**h**), and *Ankrd1* (**i**) in the RV of rats suffering from MCT-induced PH are shown. Additionally, the relative mRNA expression of *Serpine1*, *Il7r*, and *Ankrd1* in the RV of PAB rats are presented in panels **j**, **k**, and **l**, respectively. The mRNA levels were measured by qPCR, and *Gapdh* was used as an endogenous control. Data are presented as mean ± SEM and statistical significance was assessed by unpaired two-tailed t-test. (**g**, **h**, **i**): *n* (Control_2W) = 5, *n* (MCT_2W) = 4, *n* (Control_3W) = 4, *n* (MCT_3W) = 4, *n* (Control_5 W) = 4, *n* (MCT_5W-g, h) = 5, and *n* (MCT-5W-i) = 4. (**j**, **k**, and **l**): *n* (Sham_35d) = 4, *n* (PAB_35d) = 4, *n* (Sham_53d) = 4, *n* (PAB_53d) = 4.

https://doi.org/10.1038/s44161-025-00672-8

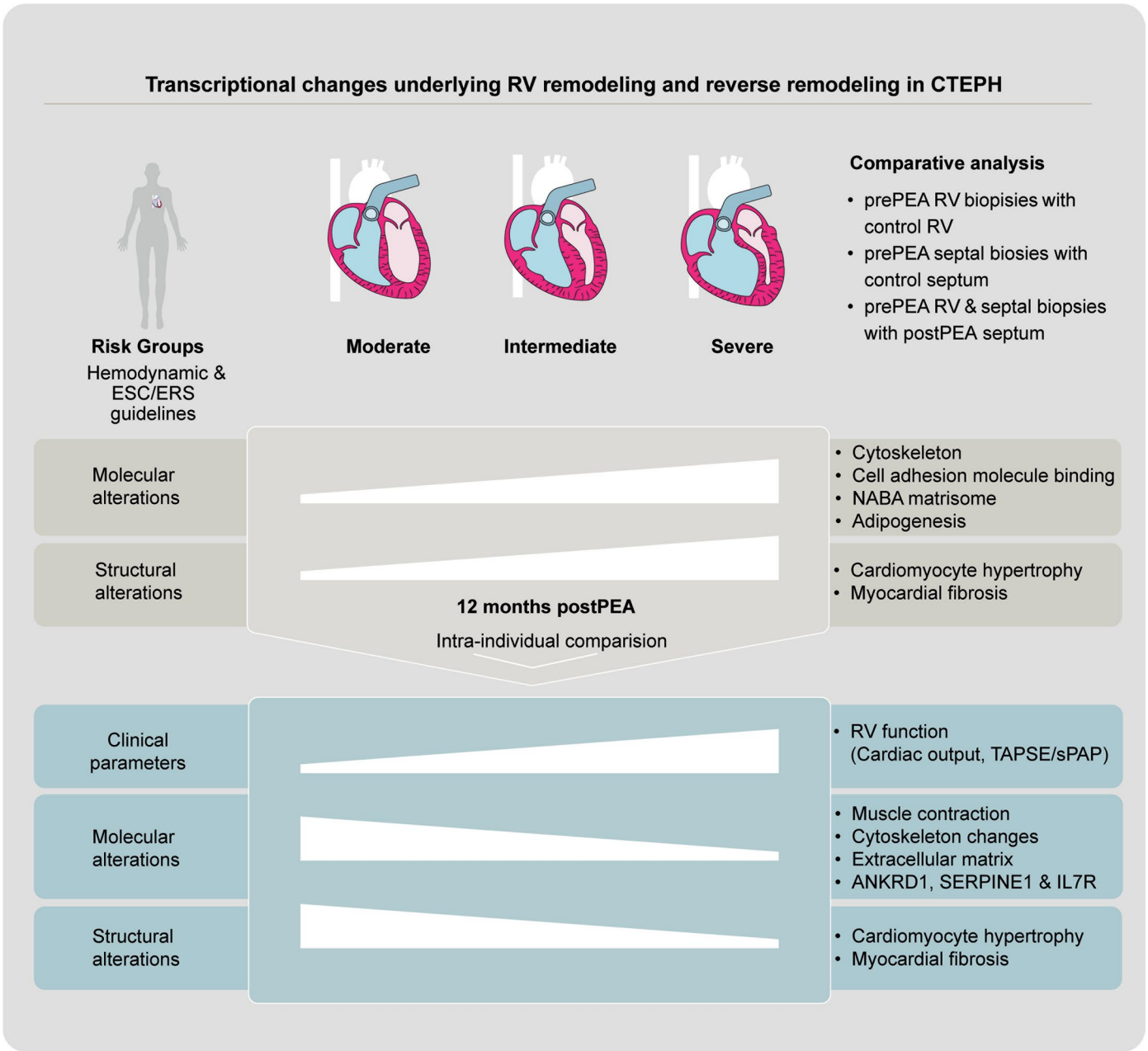

Extended Data Fig. 10 | Schematic representation of the major findings. RV, right ventricular; CTEPH, chronic thromboembolic pulmonary hypertension; PEA, pulmonary endarterectomy; ESC/ERS, European Society of Cardiology/ European Respiratory Society; TAPSE, tricuspid annular plane systolic excursion; sPAP, systolic pulmonary artery pressure; ANKRD1, Ankyrin Repeat Domain 1; SERPINE1, Serpin Family E Member 1; IL7R, Interleukin 7 Receptor. Created by Adobe Illustrator.

nature portfolio

Corresponding author(s): Christoph Liebetrau, Soni Savai Pullamsetti

Last updated by author(s): Mar 27, 2025

Reporting Summary

Nature Portfolio wishes to improve the reproducibility of the work that we publish. This form provides structure for consistency and transparency in reporting. For further information on Nature Portfolio policies, see our Editorial Policies and the Editorial Policy Checklist.

Statistics

For all statistical analyses, confirm that the following items are present in the figure legend, table legend, main text, or Methods section.

n/a	Confirmed
☐	☒ The exact sample size (*n*) for each experimental group/condition, given as a discrete number and unit of measurement
☐	☒ A statement on whether measurements were taken from distinct samples or whether the same sample was measured repeatedly
☐	☒ The statistical test(s) used AND whether they are one- or two-sided *Only common tests should be described solely by name; describe more complex techniques in the Methods section.*
☒	☐ A description of all covariates tested
☐	☒ A description of any assumptions or corrections, such as tests of normality and adjustment for multiple comparisons
☐	☒ A full description of the statistical parameters including central tendency (e.g. means) or other basic estimates (e.g. regression coefficient) AND variation (e.g. standard deviation) or associated estimates of uncertainty (e.g. confidence intervals)
☐	☒ For null hypothesis testing, the test statistic (e.g. *F*, *t*, *r*) with confidence intervals, effect sizes, degrees of freedom and *P* value noted *Give P values as exact values whenever suitable.*
☒	☐ For Bayesian analysis, information on the choice of priors and Markov chain Monte Carlo settings
☐	☒ For hierarchical and complex designs, identification of the appropriate level for tests and full reporting of outcomes
☐	☒ Estimates of effect sizes (e.g. Cohen's *d*, Pearson's *r*), indicating how they were calculated

Our web collection on statistics for biologists contains articles on many of the points above.

Software and code

Policy information about availability of computer code

Data collection	The RV and septum tissue collection for patients with CTEPH and Controls, as well as for the rat animal models are described in detail in the method part of the manuscript. The acquisition of the histopathological, immunohistological, immunofluorescence, and light microscopy images are described in the method part of the manuscript.
Data analysis	The analysis of RNA-seq and the statistical analysis of each experiment are described in detail in the method part of the manuscript. The batch correction was applied to all the RNA-seq data analyses except for Fig. 4, Extended Data Fig 4, and 5 due to the small sample size. The Human Cardiac Cell Atlas, version 2 (https://www.heartcellatlas.org/index.html) was used to identify the cell types expressing the SERPINE1, IL7R, and ANKRD1. The expression of SERPINE1, IL7R, and ANKRD1 in 704,296 individual cardiac cell types in 12 different cardiac cell types is shown. In addition, the human heart atlas data, generated using Visium technology, were used to map the expression of SERPINE1, IL7R, and ANKRD1 in three normal human right ventricle tissues (> 55 years old) in 5039 cells and in four normal human septal tissues (> 45 years old) in 8643 cells. The human protein atlas data (courtesy of Human Protein Atlas, https://www.proteinatlas.org/) were used and the correlation matrix of SERPINE1, ANKRD1, and IL7R was analyzed with three virtual reference transcripts for each cell type in myocardial tissue. In addition, the expressions of SERPINE1, ANKRD1, and IL7R and the cell type markers were mapped in different single cell type clusters of cardiac tissue and the interaction networks were examined based on the protein-protein interactions of the IntAct database for SERPINE1, IL7R and ANKRD1. To explore the transcriptional signature of LV and RV failure, we utilized two publicly available datasets (PMID: 30419824 and PMID: 33787284). The normalized read counts (PMID: 30419824) were obtained from GSE116250 and re-analyzed using the R package limma (PMID: 25605792) with default settings. For the rat animal models: mCT heart images were segmented by using Analyze 12 software (Analyze Direct, Mayo Clinic); Hemodynamic measurements: data were collected and analyzed using the PowerLab data acquisition system (MPVS-Ultra Single Segment Foundation System, AD Instruments) and LabChart 7 for Windows software.

For the PAB banding and de-banding mouse model, we re-analyzed the publicly available data set (PMID: 31738411) using Transcriptome Analysis Console (TAC, Thermo Fisher Scientific) with DEG thresholds P< 0.05 and fold change < -2 or >2.
The Venn diagrams were generated using Bioinformatics & Evolutionary Genomics (https://bioinformatics.psb.ugent.be/webtools/Venn/), and the Pathway enrichment analysis was carried out using Metascape (www.metascape.org).
The graphical elements are created with Biorender.com. and Extended Fig 10 was designed by Adobe Illustrator (v29.03, Adobe Systems Inc., San Jose, CA, USA).
To quantify the fibrosis in the RV and septum of CTEPH patients, the CellSens Standard software version 4.3 (Evident Scientific, Japan) was used. For the analysis of fibrotic area fractions, a variable number of sections per patient was analyzed to give a tissue area and the corresponding areas of the region of interest (ROI). Areas were summed up per patient, and the area fraction of the ROI per patient was calculated by dividing the summed areas (ROI area/tissue area). Differences in the area fractions between the different risk groups were analyzed in R 4.1.1 (R Core Team (2024). R: A Language and Environment for Statistical Computing. R Foundation for Statistical Computing, Vienna, Austria. https://www.R-project.org/) using a weighted generalized linear model of the quasi-binomial family, using the total tissue areas per patient as weights. The area fractions in RV and septum were compared using a paired-sample t-test on the log fractions, using the total tissue area per patient as weights.
The cross-sectional area of cardiomyocytes and tissue vascularization was assessed using Olympus CellSens Entry 2.3 software.
The clinical information of the patients with CTEPH at prePEA and postPEA in both the exploratory (at A-prePEA) and confirmatory (at B-prePEA and B-postPEA) cohorts is extensively provided in the Supplementary Tables, Extended Data Figures, and within the manuscript.
The remaining data in this study are provided in the methods, supplementary information, and Source data section of the manuscript.

For manuscripts utilizing custom algorithms or software that are central to the research but not yet described in published literature, software must be made available to editors and reviewers. We strongly encourage code deposition in a community repository (e.g. GitHub). See the Nature Portfolio guidelines for submitting code & software for further information.

Data

Policy information about availability of data

All manuscripts must include a data availability statement. This statement should provide the following information, where applicable:

- Accession codes, unique identifiers, or web links for publicly available datasets
- A description of any restrictions on data availability
- For clinical datasets or third party data, please ensure that the statement adheres to our policy

Gene expression profiling data have been deposited in the NCBI's gene expression omnibus repository (GEO) under accession number GSE249697. The dataset can be accessed at: https://www.ncbi.nlm.nih.gov/geo/query/acc.cgi?acc=GSE249697.
The code repository for the RNA-seq analysis is accessible at: https://github.com/loosolab/Code_Jafari_et_al_2024_cteph_rv_reverse_remodeling

Research involving human participants, their data, or biological material

Policy information about studies with human participants or human data. See also policy information about sex, gender (identity/presentation), and sexual orientation and race, ethnicity and racism.

Reporting on sex and gender	Both males and females have entered the study. The sex of the participants was not considered in this study, and it was defined by self-report as well as by the person who filled the study questionnaire. The sex of each patient with CTEPH in both the exploratory and confirmatory cohorts, as well as in control group, is provided in the Supplementray Table.
Reporting on race, ethnicity, or other socially relevant groupings	The reporting on race, ethnicity, or other socially relevant groupings was not considered in this study. However, all the CTEPH patients included in the study were Caucasian.
Population characteristics	The demographic characteristics and hemodynamic parameters of the patients with CTEPH in both the exploratory and confirmatory cohort are extensivly detailed in the Supplementary Tables, Extended Data, and within the manuscript. The age range of the 96 CTEPH patinets was 20.1-80.02 years. and the age range of the control group was 23.17 to 54.39 years. The CTEPH cohort consisted of 26 females and 69 males, with one patinet's sex not reported. The control group consist of 7 males and 3 females.
Recruitment	In this study, the participants who were treated by pulmonary endarterectomy (PEA) at Kerckhoff Heart and Thorax Centre between 2016 and 2020 were included. Clinical examination, echocardiography, 12-lead electrocardiogram, laboratory tests, 6-minute walk test, ventilation-perfusion-scan, computed tomography angiography, right-left-heart catheterization, and pulmonary angiography were assessed for all patients before PEA. The final diagnosis of CTEPH was made according to the guidelines in symptomatic patients after three months of effective anticoagulation, with a mean pulmonary arterial pressure (mPAP) ≥25 mmHg at rest and typical obstructive pulmonary vascular lesions on imaging diagnostics. All patients were presented in an interdisciplinary CTEPH conference to define the therapeutic concept and approve the feasibility of surgical PEA as the first-line therapy. The RV biopsies (A-prePEA, n=14 and B-prePEA, n=88) were obtained from patients who underwent the PEA. The septum biopsies (B-prePEA_septum; n = 3) were taken one day before PEA. Additionally, the septum biopsy (B-postPEA; n = 28) was taken 12 months after PEA. Tissue samples from healthy controls were collected from the same patient (n = 10) for both RV and septum. The tissue samples for control were collected in the Department of Heart Failure and Transplantology, National Institute of Cardiology, Warsaw, Poland. Healthy human hearts were obtained from organ donor patients (Control, n = 10) whose hearts were not used for transplantation due to technical reasons (e.g., donor/recipient incompatibility). The donors did not have any relevant previous cardiological history or any abnormalities in ECG and echocardiography (LV dimensions/contractility within normal ranges). The tissue samples from the ventricular free wall were taken (avoiding scarred, fibrotic, or adipose tissue,

endocardium, epicardium, or coronary vessels).

Ethics oversight

All the patients including those with CTEPH in both exploratory and confirmatory cohorts, were given written informed consent. This study was approved by the ethics board of the Justus Liebig University of Giessen (AZ 44/ 14, 144/ 11, 145/ 11, 146/ 11, 199/ 15) and is in accordance with the declaration of Helsinki. For the 10 control subjects, all experimental procedures were conducted in accordance with the ethical standards of the responsible institutional and national committee on human experimentation, as outlined in the Helsinki Declaration (1975). Written informed consent was obtained from all patients involved in the study according to the protocol approved by the Local Ethics Committees of the National Institute of Cardiology, Warsaw, Poland (approval number: IK-NPIA-0021-14/1426/18).

Note that full information on the approval of the study protocol must also be provided in the manuscript.

Field-specific reporting

Please select the one below that is the best fit for your research. If you are not sure, read the appropriate sections before making your selection.

☒ Life sciences ☐ Behavioural & social sciences ☐ Ecological, evolutionary & environmental sciences

For a reference copy of the document with all sections, see nature.com/documents/nr-reporting-summary-flat.pdf

Life sciences study design

All studies must disclose on these points even when the disclosure is negative.

Sample size

The sample sizes of the human biopsies from RV and septum, as well as the sample size for the rat RV, were determined based on the availability of the tissue samples.
In rat animal models, the sample size was pre-established based on the right ventricular systolic pressure (RVSP) and right ventricular hypertrophy (RV/LV+S).
Sample sizes for the microscopy analyses and for all the in vivo and in vitro experimental models are indicated in each figure.

Data exclusions

RNA-seq data is available for 24 septum biopsies (B-postPEA_septum), of which 22 are paired with corresponding RV biopsies. However, in our manuscript, we presented data for 21 patients [B-postPEA _septum(n=21) and B-prePEA_RV (n=21)]. Patient Nr. 96 was excluded due to its identification as an outlier in the PCA plot. The decision to exclude this patient was made to minimize data variation (Supplementray Table). For animal studies (PAB/Sham and MCT/Control rats) no exclusion criteria were pre-established. One sample from the Control_3W has been removed due to an extremely low RNA concentration.

Replication

All the biological and technical replicates related to in vitro experimental models are indicated in the respective figure legend. The rat animal studies were performed in independent biological experiments.
A total of 96 CTEPH patients included in this study, divided into an exploratory cohort (n = 14) and a confirmatory cohort (n = 89). Seven patients with RV biopsies were present in both cohorts. Additionally, One patient from the exploratory cohort, who had only a septum biopsy, was also included in the confirmatory cohort. For the RNA-seq analysis, 115 cardiac tissues from CTEPH patients were analysed, along with 10 control RV biopsies and 10 septum biopsies from the same patients.
In the exploratory cohort (A-prePEA_RV, n = 14) the RV tissue from 14 patients was sequenced. In the confirmatory cohort, out of 88 RV biopsy samples, RNA -seq was performed on 71 samples and histological analysis on 43 samples, with 26 samples overlapping between the two datasets. The allocation to RNA-seq or histology was not based on any pre-selection, bias, or stratification criteria, but rather determined solely by the amount of tissue available from each biopsy. RNA-seq data were available for 24 septum biopsies (B-postPEA_septum), of which 22 are paired with corresponding RV biopsies. However, in the manuscript, we presented data for 21 patients [B-postPEA_septum (n = 21) and B-prePEA_RV (n = 21)]. The following patients were excluded:
-Patient Nr. 96 (Pat 96-FU) was excluded due to its identification as an outlier in the PCA plot.
-Patient Nr. 83 (Pat 83-FU) was excluded due to the lack of a corresponding RV biopsy.
-Patient Nr.9 (Pat 9-FU) was excluded because there was no corresponding RV in the confirmatory cohort. This patient's RV was investigated in the exploratory cohort.
For three patients (IDs: 33, 72, and 91) the septum biopsy before PEA (B-prePEA_septum, n = 3; Pat-33-PreBL, Pat-72-PreBL, Pat-91-PreBL) and their corresponding septum biopsy after PEA (B-postPEA_septum, n = 3; Pat-33-FU, Pat-72-FU, Pat-91-FU) were sequenced.
Additionally, the RV biopsies of these patients before PEA (B-prePEA_RV, n = 3; Pat 33-BL, Pat 72-BL, Pat 91-BL and their septum biopsy (B-postPEA_septum, n = 3, Pat 33-FU, Pat 72-FU, Pat 91-FU) were sequenced.
For histological analysis, we included 47 RV biopsies (B-prePEA_RV, n = 43) with 26 RV tissues common between sequenced RV samples. 13 septum biopsies (n = 13), with 10 patients having sequenced tissue. For the vascularization, we included 7 septum biopsies from the same patients. 7 RV and 7 septum biopsies from the same patient and all these patients were common with the previously sequenced RV and septum biopsies. All the biological replicates related to the human-derived data are reported in the respective figure legend and the methods part of the manuscript.

Randomization

No randomization was applied to the participants of this study. The CTEPH patients were grouped based on their clinical parameters.
In rat animal models the animals were assigned to the study group based on the level of right ventricular hypertrophy (RV/LV+S) and right ventricular ejection fraction (RVEF).

Blinding

All the human biospecimens were processed in a standardized manner by experienced staff, who were blinded to the clinical data. The RNA-seq data were performed blinded on the RV and septum of the subjects. Histopathological, immunohistological, immunofluorescence and light microscopy procedures were also blinded during data collection and analysis.
In rat animal models, the data were acquired and analyzed in a blind fashion. Researchers were blinded to the studied groups either during

mCT acquisition and analyses or invasive hemodynamics measurements.

Reporting for specific materials, systems and methods

We require information from authors about some types of materials, experimental systems and methods used in many studies. Here, indicate whether each material, system or method listed is relevant to your study. If you are not sure if a list item applies to your research, read the appropriate section before selecting a response.

Materials & experimental systems

n/a	Involved in the study
☐	☒ Antibodies
☐	☒ Eukaryotic cell lines
☐	☐ Palaeontology and archaeology
☐	☒ Animals and other organisms
☐	☒ Clinical data
☐	☐ Dual use research of concern
☐	☐ Plants

Methods

n/a	Involved in the study
☐	☐ ChIP-seq
☐	☐ Flow cytometry
☐	☐ MRI-based neuroimaging

Antibodies

Antibodies used

CD34 monoclonal antibody Novocastra™ (1:250, # NCL-L-END, Clone QBEnd/10, Leica Biosystems, Newcastle Ltd) and the BOND Polymer Refine Detection System (# DS9800, Leica Biosystems, Newcastle Ltd)
PAI1 monoclonal antibody (SERPINE1, 1:200, #MA1-40224, Clone MA-33H1F7, ThermoFisher)
COL1A1 polyclonal antibody (1:500, #PA5-29569, ThermoFisher)
CD127 polyclonal antibody (IL7R, 1:200, #PA5-102399, ThermoFisher)
Alpha-smooth muscle actin antibody (αSMA, 1:2000, #NB300-978, Novus)
CARP polyclonal antibody (ANKRD1, 1:400, # PA5-101170, ThermoFisher)
cardiac troponin T monoclonal antibody (13-11) (cTnT, 1:1000, #MA5 12960, Clone 13-11, ThermoFisher)
secondary antibodies:
anti-mouse 594, 1:500; #A21203, ThermoFisher
anti-rabbit 488, 1:500, #A11008, ThermoFisher
anti-rabbit 594, 1:500, #A32740, ThermoFisher
anti-goat 488, 1:500, #A21467, ThermoFisher
anti-mouse 488, 1:1000, #A11029, ThermoFisher

Validation

Anti-CD34 antibody (DOI: 10.1111/j.1365-2559.1990.tb00713.x)
All the antibodies were validated by the corresponding manufacturers:
Anti-PAI1 antibody (https://www.thermofisher.com/antibody/product/PAI1-Antibody-clone-MA-33H1F7-Monoclonal/MA1-40224)
Anti-COL1A1 antibody (https://www.thermofisher.com/antibody/product/COL1A1-Antibody-Polyclonal/PA5-29569)
Anti-CD127 antibody (https://www.thermofisher.com/antibody/product/CD127-Antibody-Polyclonal/PA5-102399)
Anti-Alpha-smooth muscle actin antibody (https://www.novusbio.com/products/alpha-smooth-muscle-actin-antibody_nb300-978?srsltid=AfmBOoqZPIJVkLIAPGfiOmKAIVxk16OUTceBBwUqsRHvTKK8tfq4qucL)
Anti-CARP antibody (https://www.thermofisher.com/antibody/product/CARP-Antibody-Polyclonal/PA5-101170)
Anti-cTnT (https://www.thermofisher.com/antibody/product/Cardiac-Troponin-T-Antibody-clone-13-11-Monoclonal/MA5-12960)
Anti-mouse 594 (https://www.thermofisher.com/antibody/product/Donkey-anti-Mouse-IgG-H-L-Highly-Cross-Adsorbed-Secondary-Antibody-Polyclonal/A-21203)
Anti-rabbit 488 (https://www.thermofisher.com/antibody/product/Goat-anti-Rabbit-IgG-H-L-Cross-Adsorbed-Secondary-Antibody-Polyclonal/A-11008)
Anti-rabbit 594 (https://www.thermofisher.com/antibody/product/Goat-anti-Rabbit-IgG-H-L-Highly-Cross-Adsorbed-Secondary-Antibody-Polyclonal/A32740)
Anti-goat 488 (https://www.thermofisher.com/antibody/product/Chicken-anti-Goat-IgG-H-L-Cross-Adsorbed-Secondary-Antibody-Polyclonal/A-21467)
Anti-mouse 488 (https://www.thermofisher.com/antibody/product/Goat-anti-Mouse-IgG-H-L-Highly-Cross-Adsorbed-Secondary-Antibody-Polyclonal/A-11029)

Eukaryotic cell lines

Policy information about cell lines and Sex and Gender in Research

Cell line source(s)

Primary human cardiac fibroblasts were purchased from ScienCell Research Laboratories and primary human cardiac microvascular endothelial cells were purchased from PromoCell GmbH.

Authentication

None of the cells were authenticated.

Mycoplasma contamination	Cells were regularly tested for mycoplasma by PCR and were tested negative.
Commonly misidentified lines (See ICLAC register)	No commonly misidentified cell lines were used in this study.

Palaeontology and Archaeology

Specimen provenance	*Provide provenance information for specimens and describe permits that were obtained for the work (including the name of the issuing authority, the date of issue, and any identifying information). Permits should encompass collection and, where applicable, export.*
Specimen deposition	*Indicate where the specimens have been deposited to permit free access by other researchers.*
Dating methods	*If new dates are provided, describe how they were obtained (e.g. collection, storage, sample pretreatment and measurement), where they were obtained (i.e. lab name), the calibration program and the protocol for quality assurance OR state that no new dates are provided.*

☐ Tick this box to confirm that the raw and calibrated dates are available in the paper or in Supplementary Information.

Ethics oversight	*Identify the organization(s) that approved or provided guidance on the study protocol, OR state that no ethical approval or guidance was required and explain why not.*

Note that full information on the approval of the study protocol must also be provided in the manuscript.

Animals and other research organisms

Policy information about studies involving animals; ARRIVE guidelines recommended for reporting animal research, and Sex and Gender in Research

Laboratory animals	The RV tissue was obtained from pulmonary artery banding (PAB)/Sham operated and monocrotaline (MCT)-injected/Control rats. The strain of the animals was Sprague-Dawley rats. In PAB/Sham rat models the hemodynamics measurements and RV tissues were obtained from animals on days 35 and 53 after PAB/sham operation. In MCT/Control rats the hemodynamics measurements and RV tissues collection were performed after 2, 3, and 5 weeks of MCT injection.
Wild animals	This study did not involve wild animals.
Reporting on sex	The finding of this study was applied to only male rat animal models.
Field-collected samples	This study did not involve field-collected samples.
Ethics oversight	The animal study protocols were conducted in accordance with the National Institute of Health Guidelines on the Use of Laboratory Animals. The study protocols were approved by the University Animal Care Committee and the Federal Authorities for Animal Research of the Regierungspräsidium Giessen (GI 20/10 Nr G92/2017 RP Giessen), Hessen, Germany.

Note that full information on the approval of the study protocol must also be provided in the manuscript.

Clinical data

Policy information about clinical studies

All manuscripts should comply with the ICMJE guidelines for publication of clinical research and a completed CONSORT checklist must be included with all submissions.

Clinical trial registration	Not applicable, as the study was observational.
Study protocol	The study population and clinical work-up of this study are explained in the methods section of the manuscript. For the patients with CTEPH the study was approved by the ethics board of the Justus Liebig University of Giessen (AZ 44 / 14, 144 / 11, 145 / 11, 146 / 11, 199 / 15) and in accordance with the declaration of Helsinki. For the control participants, the study protocol was approved by the Local Ethics Committees of the National Institute of Cardiology, Warsaw, Poland (approval number: IK-NPIA-0021-14/1426/18).
Data collection	The human RV and septum acquisition from the RV and septum of patients with CTEPH and control subjects were explained in detail in the Methods section of the revised manuscript.
Outcomes	In this prospective study, patients with CTEPH, are divided into two distinct cohorts: an exploratory cohort and a confirmatory cohort. The patients in each cohort were risk stratified based on their clinical parameters and the European Society of Cardiology (ESC) and the European Respiratory Society (ERS) guidelines using a three-strata model into a moderate, intermediate, and severe risk group. In addition, this study included a subgroup of patients, with postPEA septum biopsies collected 12 months after PEA, and all were matched with prePEA counterparts. Additionally, in the confirmatory cohort, in the subgroup of 3 patients, with the biopsies before PEA from RV (B-prePEA_RV, n = 3) and 12 months after PEA from the septum (B-postPEA_septum, n = 3), the biopsy was obtained from the septum before PEA (B-prePEA_septum, n = 3). The clinical parameters of all the patients with CTEPH are shown in the Supplementary Tables.

Dual use research of concern

Policy information about dual use research of concern

Hazards

Could the accidental, deliberate or reckless misuse of agents or technologies generated in the work, or the application of information presented in the manuscript, pose a threat to:

No	Yes	
☐	☐	Public health
☐	☐	National security
☐	☐	Crops and/or livestock
☐	☐	Ecosystems
☐	☐	Any other significant area

Experiments of concern

Does the work involve any of these experiments of concern:

No	Yes	
☐	☐	Demonstrate how to render a vaccine ineffective
☐	☐	Confer resistance to therapeutically useful antibiotics or antiviral agents
☐	☐	Enhance the virulence of a pathogen or render a nonpathogen virulent
☐	☐	Increase transmissibility of a pathogen
☐	☐	Alter the host range of a pathogen
☐	☐	Enable evasion of diagnostic/detection modalities
☐	☐	Enable the weaponization of a biological agent or toxin
☐	☐	Any other potentially harmful combination of experiments and agents

Plants

Seed stocks	*Report on the source of all seed stocks or other plant material used. If applicable, state the seed stock centre and catalogue number. If plant specimens were collected from the field, describe the collection location, date and sampling procedures.*
Novel plant genotypes	*Describe the methods by which all novel plant genotypes were produced. This includes those generated by transgenic approaches, gene editing, chemical/radiation-based mutagenesis and hybridization. For transgenic lines, describe the transformation method, the number of independent lines analyzed and the generation upon which experiments were performed. For gene-edited lines, describe the editor used, the endogenous sequence targeted for editing, the targeting guide RNA sequence (if applicable) and how the editor was applied.*
Authentication	*Describe any authentication procedures for each seed stock used or novel genotype generated. Describe any experiments used to assess the effect of a mutation and, where applicable, how potential secondary effects (e.g. second site T-DNA insertions, mosiacism, off-target gene editing) were examined.*

ChIP-seq

Data deposition

☐ Confirm that both raw and final processed data have been deposited in a public database such as GEO.

☐ Confirm that you have deposited or provided access to graph files (e.g. BED files) for the called peaks.

Data access links *May remain private before publication.*	*For "Initial submission" or "Revised version" documents, provide reviewer access links. For your "Final submission" document, provide a link to the deposited data.*
Files in database submission	*Provide a list of all files available in the database submission.*
Genome browser session (e.g. UCSC)	*Provide a link to an anonymized genome browser session for "Initial submission" and "Revised version" documents only, to enable peer review. Write "no longer applicable" for "Final submission" documents.*

Methodology

Replicates	*Describe the experimental replicates, specifying number, type and replicate agreement.*
Sequencing depth	*Describe the sequencing depth for each experiment, providing the total number of reads, uniquely mapped reads, length of reads and whether they were paired- or single-end.*
Antibodies	*Describe the antibodies used for the ChIP-seq experiments; as applicable, provide supplier name, catalog number, clone name, and lot number.*
Peak calling parameters	*Specify the command line program and parameters used for read mapping and peak calling, including the ChIP, control and index files used.*
Data quality	*Describe the methods used to ensure data quality in full detail, including how many peaks are at FDR 5% and above 5-fold enrichment.*
Software	*Describe the software used to collect and analyze the ChIP-seq data. For custom code that has been deposited into a community repository, provide accession details.*

Flow Cytometry

Plots

Confirm that:

☐ The axis labels state the marker and fluorochrome used (e.g. CD4-FITC).

☐ The axis scales are clearly visible. Include numbers along axes only for bottom left plot of group (a 'group' is an analysis of identical markers).

☐ All plots are contour plots with outliers or pseudocolor plots.

☐ A numerical value for number of cells or percentage (with statistics) is provided.

Methodology

Sample preparation	*Describe the sample preparation, detailing the biological source of the cells and any tissue processing steps used.*
Instrument	*Identify the instrument used for data collection, specifying make and model number.*
Software	*Describe the software used to collect and analyze the flow cytometry data. For custom code that has been deposited into a community repository, provide accession details.*
Cell population abundance	*Describe the abundance of the relevant cell populations within post-sort fractions, providing details on the purity of the samples and how it was determined.*
Gating strategy	*Describe the gating strategy used for all relevant experiments, specifying the preliminary FSC/SSC gates of the starting cell population, indicating where boundaries between "positive" and "negative" staining cell populations are defined.*

☐ Tick this box to confirm that a figure exemplifying the gating strategy is provided in the Supplementary Information.

Magnetic resonance imaging

Experimental design

Design type	*Indicate task or resting state; event-related or block design.*
Design specifications	*Specify the number of blocks, trials or experimental units per session and/or subject, and specify the length of each trial or block (if trials are blocked) and interval between trials.*
Behavioral performance measures	*State number and/or type of variables recorded (e.g. correct button press, response time) and what statistics were used to establish that the subjects were performing the task as expected (e.g. mean, range, and/or standard deviation across subjects).*

Acquisition

Imaging type(s) *Specify: functional, structural, diffusion, perfusion.*

Field strength *Specify in Tesla*

Sequence & imaging parameters *Specify the pulse sequence type (gradient echo, spin echo, etc.), imaging type (EPI, spiral, etc.), field of view, matrix size, slice thickness, orientation and TE/TR/flip angle.*

Area of acquisition *State whether a whole brain scan was used OR define the area of acquisition, describing how the region was determined.*

Diffusion MRI ☐ Used ☐ Not used

Preprocessing

Preprocessing software *Provide detail on software version and revision number and on specific parameters (model/functions, brain extraction, segmentation, smoothing kernel size, etc.).*

Normalization *If data were normalized/standardized, describe the approach(es): specify linear or non-linear and define image types used for transformation OR indicate that data were not normalized and explain rationale for lack of normalization.*

Normalization template *Describe the template used for normalization/transformation, specifying subject space or group standardized space (e.g. original Talairach, MNI305, ICBM152) OR indicate that the data were not normalized.*

Noise and artifact removal *Describe your procedure(s) for artifact and structured noise removal, specifying motion parameters, tissue signals and physiological signals (heart rate, respiration).*

Volume censoring *Define your software and/or method and criteria for volume censoring, and state the extent of such censoring.*

Statistical modeling & inference

Model type and settings *Specify type (mass univariate, multivariate, RSA, predictive, etc.) and describe essential details of the model at the first and second levels (e.g. fixed, random or mixed effects; drift or auto-correlation).*

Effect(s) tested *Define precise effect in terms of the task or stimulus conditions instead of psychological concepts and indicate whether ANOVA or factorial designs were used.*

Specify type of analysis: ☐ Whole brain ☐ ROI-based ☐ Both

Statistic type for inference *Specify voxel-wise or cluster-wise and report all relevant parameters for cluster-wise methods.*

(See Eklund et al. 2016)

Correction *Describe the type of correction and how it is obtained for multiple comparisons (e.g. FWE, FDR, permutation or Monte Carlo).*

Models & analysis

n/a	Involved in the study
☐	☐ Functional and/or effective connectivity
☐	☐ Graph analysis
☐	☐ Multivariate modeling or predictive analysis

Functional and/or effective connectivity *Report the measures of dependence used and the model details (e.g. Pearson correlation, partial correlation, mutual information).*

Graph analysis *Report the dependent variable and connectivity measure, specifying weighted graph or binarized graph, subject- or group-level, and the global and/or node summaries used (e.g. clustering coefficient, efficiency, etc.).*

Multivariate modeling and predictive analysis *Specify independent variables, features extraction and dimension reduction, model, training and evaluation metrics.*